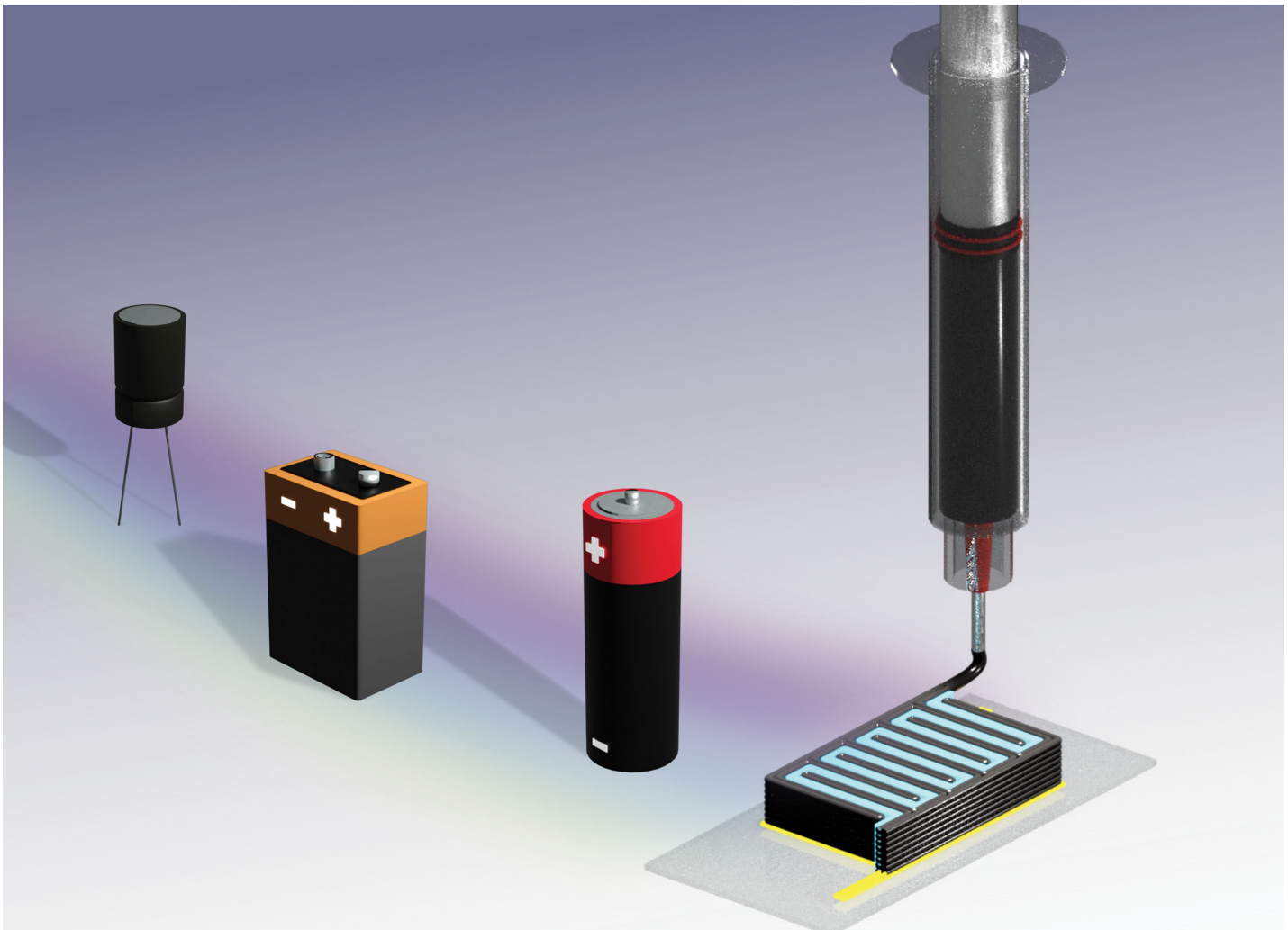

Showcasing research from Dr Cecilia Mattevi's laboratory, Department of Materials, Imperial College London, UK.

Direct ink writing of energy materials

Direct Ink Writing, one of the leading extrusion-based 3D printing processes, holds great potential for the sustainable fabrication of energy devices with arbitrary architectures. Ink formulation is a crucial step in the manufacturing of electrochemically efficient and mechanically robust devices, offering the possibility to boost the performance and the durability of energy systems. In this work, we discuss the ink formulation approaches that have been proposed to print energy materials *via* Direct Ink Writing, providing insights into the integration of different materials to manufacture all-printed energy systems in a single production process.

As featured in:

See C. Mattevi *et al.*, *Mater. Adv.*, 2021, **2**, 540.

ROYAL SOCIETY OF CHEMISTRY

rsc.li/materials-advances

Registered charity number: 207890

Materials Advances

ROYAL SOCIETY OF CHEMISTRY

REVIEW

View Article Online
View Journal | View Issue

Cite this: *Mater. Adv.*, 2021, **2**, 540

Direct ink writing of energy materials

S. Tagliaferri, A. Panagiotopoulos and C. Mattevi *

Received 30th September 2020,
Accepted 7th November 2020

DOI: 10.1039/d0ma00753f

rsc.li/materials-advances

3D printing is a promising technique for the sustainable fabrication of energy devices with arbitrary architectures. Extrusion-based 3D printing, called direct ink writing, is increasingly used for the manufacturing of batteries, supercapacitors and catalytic systems. In order to obtain mechanically stable and functional devices, inks formulation must meet stringent criteria for printability, that are usually expressed in terms of rheological properties. Inks are rheologically complex fluids, in which the electroactive materials are mixed with additives and solvents to form an extrudable and self-standing paste. The ink formulation process plays a key role in tuning the rheology and the functional properties of the printed device. In this review, inks formulation, rheological characteristics and device performance are critically discussed, providing insights into the rheology-printability and formulation–functional properties relationships. The main strategies that have been proposed to obtain printable inks from energy materials are reviewed. The role played by the different ink components to achieve the target rheology is contextualized and the integration of different inks into an all-printed device is discussed. Finally, an outlook on the future challenges and opportunities for the DIW of energy materials is provided with the view that general formulations which do necessitate thermal post processing could widen the opportunities of this manufacturing technique enabling the use for large scale production of energy devices.

Introduction

There is an increasing demand in developing sustainable manufacturing techniques which can enable an automated fabrication of a defined number of products on demand, at comparable cost of the conventional serial production routes. The advantage would be to make goods production more sustainable, minimizing the waste and energy involved. This would lead to a paradigm shift in the current industry, where advanced manufacturing techniques would then establish a new system of large-scale production. 3D printing is an additive manufacturing technique which would respond to this new demand of societal sustainability. The use of 3D printing to produce functional devices is rapidly growing, with an increasing number of publications on printed sensors and electrochemical devices every year.[1–3]

In specific, printing techniques offer significant advantages over existing methods for the fabrication of electrochemical devices for energy storage and conversion in small dimensions. These advantages include: (1) the production of structures with arbitrary geometry, lateral extension and thickness; (2) tunable composition and physical properties of the printed devices and (3) low manufacturing costs and reduced material waste, permitted by the additive nature of the process. Additionally, 3D printing presents good compatibility with curved and flexible substrates, such as plastic and paper,[2] as the process is usually performed in air and at room temperature.

These unique features make 3D printing a valuable manufacturing technique for the production of three-dimensional energy devices in miniaturized dimensions. Three-dimensional structures with tailored geometry can efficiently enhance the performance and durability of batteries and supercapacitors, allowing larger amounts of active material per footprint area, and promote short and uninterrupted diffusive paths for the efficient transport of electrons, ions and charge–discharge products.[4] Additionally, programmable designs can minimize the mechanical strain that arises during cycling, challenging the structural integrity of the electrodes, and enhance the surface area accessible to charge storage processes.[5,6] As a result, 3D printed batteries and supercapacitors often exhibit superior performance than bulk structures.[6]

3D printing can also enhance the performance of catalytic systems, that are often limited by sluggish mass transport and low accessibility to the active surface.[7] When 3D printing is combined with templating techniques, hierarchical structures with controlled micro- and macroporosity can be obtained, increasing the catalytic performance.[8] Contrary to templating methods, 3D printing allows to pattern the material structure in a completely deterministic way, broadening the possibility of structural optimization.

Recent reviews have discussed the advantages of printing energy devices, comparing the benefits and limitations of different

Department of Materials, Imperial College London, London SW7 2AZ, UK.
E-mail: c.mattevi@imperial.ac.uk

printing techniques.[9–14] Egorov *et al.*,[13] in particular, have assessed the suitability of 3D printing techniques for energy storage applications considering five parameters: prototyping speed, volume, manufacturing cost, quality of the printed structure and possibility to print multiple materials.

The principal aim of this review is to discuss the fabrication of energy devices *via* Direct Ink Writing (DIW), placing emphasis on the formulation of printable inks for energy applications. Firstly, the advantages of DIW over the other 3D printing techniques to produce three-dimensional energy devices are presented. Secondly, we provide detailed insights into the concept of printability for DIW, examining how optimal ink extrusion and deposition can be achieved, ensuring the formation of a highly performing functional electrode. We then critically discuss the strategies employed to formulate inks based on solid-state materials that are relevant for energy applications, and the challenges in the field. We ultimately promote a comprehensive approach to prototyping that can lead to relying on DIW for the manufacturing of the entire device, paving the way towards the adaptation of a new industrially scalable approach to energy systems.

The wide spectrum of 3D printing techniques

A wide variety of 3D printing techniques has been recently employed to fabricate three-dimensional energy devices from digital designs (Fig. 1). Printed devices are usually obtained *via* the deposition and consolidation of subsequent layers of material, although the printable materials, the building speed, the printing resolution and the manufacturing cost strongly depend on the specific process considered.

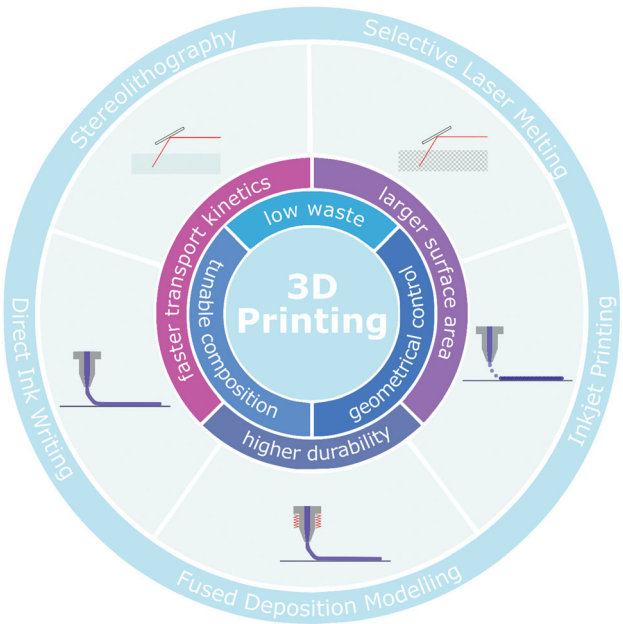

Fig. 1 Advantages of 3D printing for energy devices and main 3D printing techniques.

3D printing processes based on the consolidation of sequential layers of powder, such as selective laser melting and selective laser sintering,[15,16] are usually compatible with large-volume printing. However, their high cost, rough surface finish, and difficulty to recycle the unsintered powders have limited their application for energy devices.[10,11] In contrast, stereolithography and other lithographic processes[17,18] ensure high resolution and good shape definition, since they are based on the layer-by-layer polymerization process of a photosensitive resin under irradiation. Arbitrarily complex shapes can be obtained through these techniques, although some of them require the use of a lithographic mask, that reduces the number of obtainable architectures and increases the production costs.[14] Nevertheless, stereolithography has seen limited applications for energy devices, owing to the constrained use of photocurable polymers in the formulations and to the low printing speed, around a few millimetres per hour in the vertical direction.[9,10,19]

Inkjet printing has been extensively used for the fabrication of electronic devices.[20,21] It is based on the ejection of ink droplets from a printing head, *via* a thermal or piezoelectric mechanism, to form a continuous line with good spatial resolution (<25 μm) onto the substrate.[22,23] This technique allows the deposition of a variety of different inks, which are usually characterized by high fluidity to avoid nozzle clogging. As a consequence, the concentration of active materials is usually around a few mg mL^{-1},[24,25] which is considerably lower than the inks used in other printing techniques, such as direct ink writing.[26] Inkjet printing can be assimilated to the family of 3D printing processes because it offers a certain degree of control over the thickness of the printed features, which usually ranges between tens and hundreds of microns.[23,27] Nonetheless, three-dimensional architectures presenting voids, load-bearing elements and unsupported overhangs cannot be fabricated *via* this process.[28]

In fused deposition modelling a filament of thermoplastic polymer is heated over its glass transition temperature and extruded through the printing head.[29,30] This process presents low costs and it ensures high printing speed. Currently, it is not particularly suited for energy storage applications, since the active materials must be blended with large amounts of thermoplastic polymers, thus compromising the functional properties of the printed structure. In addition, the printing resolution is limited to hundreds of microns,[31] hindering the fabrication of miniaturized devices.[9]

Direct ink writing[32] has recently gained significant attention for energy applications. This printing process is unique in its ability to extrude continuous filaments at room temperature, since the solidification of the printed filament does not rely on temperature but on the rheological properties of the ink. The maximum resolution achievable depends on the diameter of the extrusion nozzle and on the flow behaviour of the ink. In particular, solid features with a lateral dimension smaller than 1 μm can be printed using nozzles with a diameter of ~600 nm,[33–35] indicating the suitability of this process to

obtain miniaturized devices with high form factors. Additionally, a wide variety of materials can be printed *via* direct ink writing, including ceramics, polymers and metals. The multimaterial capability of this printing technique allows the fabrication of all-printed devices that can be readily integrated with external electronics, reducing the cost and complexity of the manufacturing process.

Although DIW holds great potential for the fabrication of energy devices, the optimization of ink rheology to achieve suitable printability and desirable functional properties is a pressing challenge. Most publications about direct ink writing for energy applications place a great deal of attention on the choice of the active materials and on the electrochemical properties of the final device. Nonetheless, control over the rheology of the inks, obtained by carefully adjusting the ink composition, is fundamental to attain the desired geometry, resolution and functionality of the device and to ultimately achieve good performance.

A wide variety of strategies have been presented in recent literature to formulate printable inks from energy materials. However, a comprehensive review that discusses the advantages and limitations of the different strategies, and how they can be combined to print multimaterial devices, is currently missing. The main ink formulation strategies, together with the concept of printability for DIW, will be critically presented in the following discussion.

Rheology of inks for energy devices

Printability of energy materials

The DIW deposition process can be divided into three steps (Fig. 2): (1) the flow of the ink through the syringe barrel and printing nozzle; (2) the ejection of the ink from the nozzle and (3) the deposition of the ink onto the underlaying printed layers. During each one of these fundamental steps, the ink should meet specific requirements to be printable. It has often been highlighted that the concept of printability is not universal, and it is strictly related to the use and application of the printed object.[36] Hence, this section will discuss the printability of inks for the fabrication of energy devices, and review how printability has been effectively linked to the rheological properties of the ink. In particular, we will present the requirements to print self-supported device components, such as battery electrodes and cell casing. Different ink properties might be required to manufacture non-structural elements, notably the electrolyte and the current collector. Further discussion on the fabrication of these components will be presented in the section dedicated to multimaterial printing.

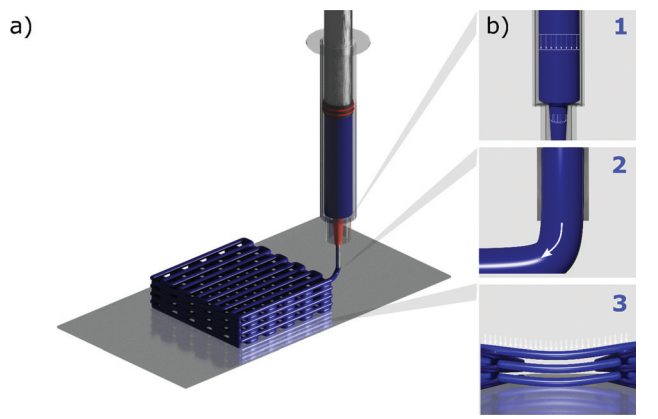

Fig. 2 (a and b) Schematic showing the main steps of the printing process: flow of the ink inside the syringe barrel and nozzle (1), ejection of the ink from the nozzle (2) and deposition onto the substrate to form a self-standing structure (3).

As a very general definition, an ink is considered printable if it can be extruded through a selected nozzle in the form of a continuous filament, able to build structures that accurately replicate the digital model. The morphology of the printed structure should be retained after deposition, drying and post-processing.[37] In recent times there has been a significant interest in miniaturized electrochemical systems, especially microsupercapacitors[38,39] and microbatteries.[40,41] In order to print devices with miniaturized footprint area, the physical properties of the inks must be carefully tailored, and inks that have been designed for large-scale systems might prove unsuitable for microfabrication, owing to clogging during the first steps of the printing process. In particular, the ink should be able to flow smoothly, without forming large and hard agglomerates that can jam the deposition nozzle.[32,42] The flow behaviour of the ink should also promote moderate extrusion pressures, especially when using micronozzles.[43,44] This requirement is particularly important to fabricate miniaturized devices, since the diameter of the deposition nozzle is the main factor that controls the printing resolution.[43] From a rheological perspective, a shear thinning behaviour is usually sought to meet these criteria.[43,45,46] Shear-thinning, *i.e.* a reduction of viscosity over increasing shear rate, can favour the flow of the ink through capillary nozzles and reduce the extrusion pressure, ensuring ink extrudability.[46]

When the ink is ejected from the printing head, it must quickly turn from a shear-thinning fluid into a solid-like material to retain its shape after deposition.[32] Inks employed in direct ink writing are usually yield stress fluids,[32,36,47] which behave as elastic or viscoelastic solids under a threshold value of stress, known as the yield stress, while they flow when the yield stress is exceeded. Ideally, the properties of a yield-stress ink should only depend on the instantaneous rate at which it is sheared, so that its structural integrity is immediately retrieved when it stops flowing. However, ink properties are often influenced by shear history as well, indicating that inks are thixotropic.[36,44,46,48] In thixotropic materials the rest properties are only retrieved after a finite recovery time, which can be relatively long when compared to the deposition time,[46,49] and microstructural changes may still be taking place after the deposition of the ink.[46] During DIW, the recovery process should be adequately fast in order to achieve good shape accuracy and avoid slumping of the structure. It is worth noting that when the ink leaves the nozzle it is not yet completely at rest. Although it is not subjected to the high shear stresses experienced during flow anymore, the ink filament still goes through bending and

stretching before final deposition. The degree of ink stretching can be controlled by altering the ratio between the extrusion rate and printing speed. In particular, Yuk *et al.*[50] have shown that the stretching experienced during extrusion can be tailored to print structures with a finer resolution than the nozzle diameter. This technique is potentially promising for the printing of miniaturized electronics, but it has only been applied to polymeric inks so far.

When the deposition process is complete, the printed structure must retain its shape until full solidification has occurred, usually by solvent removal. The rheological properties required during this final step of the printing process are highly dependent on the design of the structure. The main designs used for printed electrodes, namely the woodpile, the interdigitated and the compact design, pillars and fibres, are presented in Fig. 3. Woodpile and interdigitated electrodes are commonly employed in printed batteries and supercapacitors.[51–53] The former consists of alternated layers of equally spaced rods, each perpendicular to the rods of the previous layer, forming macroscopic channels that promote electrolyte infiltration and ion diffusion.[52] Woodpile structures are also used as electrodes for electrocatalysis, since they present high surface area and good mechanical stability.[8,54] In contrast, interdigitated electrodes present arrays of interdigital fingers, printed side by side on the same substrate. Several authors[39,41,55,56] have discussed the advantages of the interdigitated geometry for energy storage systems. These include shorter diffusion length, smaller distance between the electrodes and the absence of a separator, which are beneficial to the performance of miniaturized and integrated energy devices.[56] The third and the fourth electrodes designs are fibres and pillars. The former is gaining importance in flexible and wearable systems and there are a few examples of the realization of such design.[57] In contrast, the fabrication of pillar structures *via* DIW has not been studied extensively for energy devices yet, owing to the uncommon rheological requirements necessary to avoid lateral instabilities, though micropillars are relatively common in non-printed three-dimensional batteries.[58–60] Finally, compact and space-filling structures can also be obtained with 3D printing,[61] however they are not very common in energy storage and conversion devices, where high surface area is usually sought to enhance transport.

The main geometrical features presented by the designs in Fig. 3 are spanning elements (woodpile structure) and vertical walls, which can be either made of stacked filaments (interdigitated structure), or of a single continuous filament (pillar structure). After printing, the ink should possess suitable rheology to prevent the slumping of the stacked filaments under their own weight and under the effect of capillary forces, and it should be able to minimize the bending of spanning elements.[62,63] In particular, a high storage modulus at rest is necessary to limit bending of suspended parts, whereas a high yield stress prevents the structure from collapsing.[36,62,63] It is worth noting that space-filling structures would require a lower storage modulus to avoid that the excessive elasticity may hinder the fusion of neighbouring filaments.[64,65] However, since dense and thick structures are rarely employed in energy storage, a very high storage modulus ($>10^4$ Pa) is usually desirable.

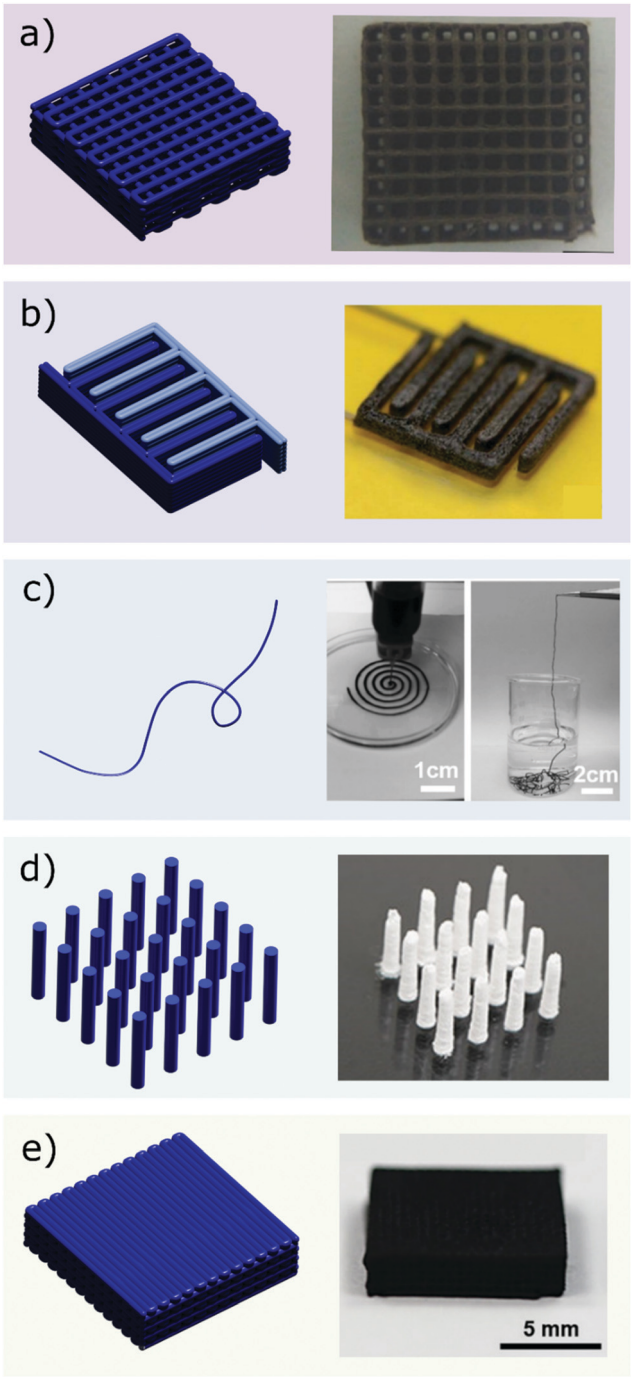

Fig. 3 Common 3D designs used in printed energy devices: (a) woodpile (adapted with permission from ref. 74, Copyright 2018 John Wiley and Sons), (b) interdigitated (adapted with permission from ref. 109, Published by The Royal Society of Chemistry), (c) fibres (adapted with permission from ref. 57, Copyright 2017 John Wiley and Sons), (d) pillars (adapted with permission from ref. 60, Copyright 2019 American Chemical Society) and (e) compact structures (adapted with permission from ref. 61, Copyright 2018 John Wiley and Sons).

Structure of printable inks

In order to meet the rheological criteria presented above, inks should behave as yield-stress fluids with a marked shear thinning during flow and a fast recovery of their elastic properties after

shear. We will now examine ink microstructures that have been proven to satisfy these conditions, promoting favourable rheological properties during printing. In this regard, Nelson *et al.*[66,67] have discussed the design of yield stress fluids, providing guidelines to select the right microstructure to meet functional requirements, such as printability.

Yield-stress materials used as inks in 3D printing include polymeric gels, emulsions and colloidal dispersions (Fig. 4), which are all characterized by a jammed microstructure arising from soft interactions between their constitutive elements.[68] The interactions in the jammed materials are usually either attraction- or repulsion-dominated,[66] although the two types of interactions might coexist in more complex systems.[69] The jammed structure is broken down when a sufficiently high stress is applied to the material, causing the typical yielding behaviour.[68]

Among yield-stress fluids, colloidal suspensions can be taken as model systems to describe the microstructural evolution during the printing process, since they have been widely studied as inks for printed ceramic architectures.[44] Colloidal dispersions that present a yield stress can be divided into two types: jammed colloidal glasses and colloidal gels. In the first ones, the colloidal particles interact through repulsive forces, while the second ones consist of a percolated network of attracting particles.[67] In particular, in colloidal glasses the particles are trapped by cages formed by their nearest neighbours, and the repulsive potential arise from steric stabilization which prevents aggregation due to van der Waals interactions.[70] The properties of colloidal glasses may vary significantly with small fluctuations in concentration and particles can very easily clog microchannels. For this reason, colloidal gels are considered more suitable for DIW than colloidal glasses.[71] In colloidal gels the attractive interactions can either arise from hydrogen bonds between hydrogen-containing moieties or from electrostatic forces between charged particles and bridging ions.[44,72] When the material yields under stress, the interparticle bonds are broken and large clusters of particles gain mobility (Fig. 5). With increasing stress, the clusters of particles are fragmented into smaller flocs, determining the shear-thinning behaviour that is commonly observed in these materials.[49,71] Finally, after flow cessation, bonds between flocs rebuild, forming larger aggregates and eventually a network.[46]

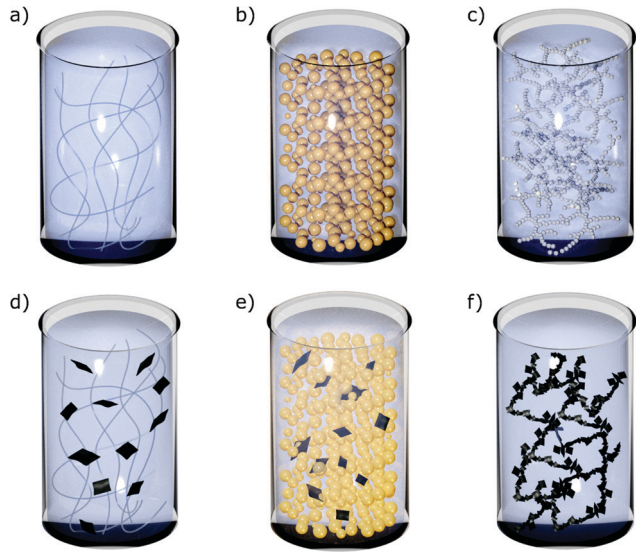

Fig. 4 Schematics showing typical yield-stress fluids used as inks in direct ink writing: (a) polymeric gels, (b) emulsions and (c) colloidal dispersions. Materials for energy storage can be added to these formulations to obtain functional inks (d–f).

This qualitative description is useful to understand the behaviour of most inks for energy devices, which usually rely on attractive interactions between their components, presenting a microstructure similar to colloidal gels. In inks for energy devices, the percolated network can be either directly formed by the particles of active material,[73,74] or be promoted by the addition of inactive additives.[75,76] The properties of the attractive networks can be strongly affected by the shear history, causing a thixotropic behaviour that might be detrimental for printing.

Rheological models for ink printability

Several mathematical models have been proposed to translate the concept of printability in measurable quantities. The flow behaviour of inks for DIW is usually described using the Herschel–Bulkley model:[32,68]

$$\tau = \tau_y + K\dot{\gamma}^n$$

where τ is the shear stress, K the viscosity parameters, n the flow index and τ_y the yield stress. This empirical model assumes that the ink cannot flow for values of stress lower than τ_y, and that it presents a rate-dependent viscosity during flow (either shear-thinning if $n < 1$, or shear-thickening if $n > 1$).

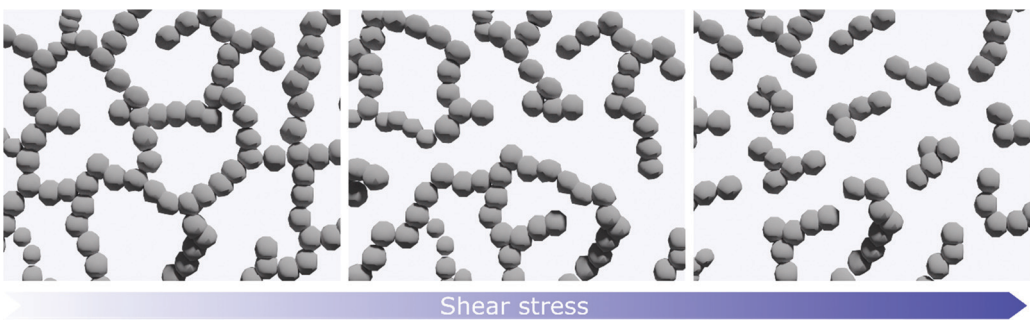

Fig. 5 Microstructure evolution inside a colloidal gel made of a percolated particle network at increasing level of stress.

The Herschel–Bulkley parameters (*i.e.* n, K and τ_y) have been used to predict the shear rate profile and the pressure gradient required to print ceramic inks *via* DIW.[63] The Herschel–Bulkley model was also implemented in finite-element numerical simulation to predict the flow profiles of colloidal inks in microchannels.[77,78] Although this model is widely used, it is unable to describe the transient destruction and restructuring process taking place in yield-stress materials during flow, and their elastic or viscoelastic behaviour below the yield stress.[68] In addition, the parameter K has non-integer dimensions (Pa s^n) that depend on the flow index n, and does not allow the direct comparison of different inks. Alternative formulations of the Herschel–Bulkley model based on more physically-meaningful parameters have been consequently proposed.[66]

A simple model to describe the thixotropy of DIW inks was introduced by Zhu *et al.*[46] to study the rheology of alumina pastes. It is based on the definition of a structure parameter λ, which represents the degree of aggregation of primary flocs in the ink. When $\lambda = 1$ the gel is completely structured, and a sample-spanning network exists. Assuming that the destruction rate is proportional to λ, and that the reconstruction rate to $1 - \lambda$, a kinetic equation that describes the time evolution of the structure during flow was derived. The elastic modulus and viscosity were then related to the structure parameter λ, and a constitutive equation for the fluid was obtained. It was then shown how the constitutive equation parameters, describing the material viscosity, elasticity and evolution kinetics, could be controlled by altering the system composition.

M'Barki *et al.*[62] introduced a quantitative criterion to establish the minimum yield stress necessary to avoid slumping under the effect of gravity and capillary forces. It can be expressed as:

$$\sigma_y^{dyn} \geq \gamma R^{-1} + \rho g h$$

where σ_y^{dyn} is the dynamic yield stress, γ the suspension surface tension, R the nozzle diameter and $\rho g h$ represents the gravitational force acting on the printed filament. They also showed that this criterion describes printability better than models purely based on gravitational slumping. Simple mathematical models have also been employed to describe the deformation of printed structures at rest. Smay *et al.*[63] applied the elastic beam theory to spanning ink filaments to determine the minimum storage modulus required to have a sufficiently small deflection. Setting the maximum acceptable deflection equal to 5% of the nozzle diameter, this useful scaling relationship was obtained:

$$G' \geq 1.4\gamma \left(\frac{L}{D}\right)^4 D$$

where L is the length of the spanning element, D its diameter and γ the specific weight of the ink. When deriving this equation, it was assumed that the ink is incompressible (*i.e.* has a Poisson ratio of 0.5), which might not hold true for all formulations. Applying this equation to the woodpile structure in Fig. 3 and measuring the density of the inks, it is possible to calculate the minimum storage modulus to print an electrode with good shape fidelity. This simple elastic model was then refined to consider viscoelastic effects on the shape of spanning elements.[79] Similarly, a linear viscoelastic model was used by Cao *et al.*[76] to determine the range of printability of inks for Li-ion batteries.

Rheological characterization

The rheological properties of inks for DIW are usually assessed *via* shear rheology using a rotational rheometer (Fig. 6).[80] The most common rheological tests are flow ramps, which allow to evaluate the degree of shear thinning of inks,[63] and oscillatory tests, which give information on the viscoelastic properties at rest.[33] In most of the publications on printed energy materials the yield stress is also determined from oscillatory tests, as the value of stress at which the storage modulus equals the loss modulus.[61,81] This method appears to be quick and reliable, although it provides higher values than the Herschel–Bulkley fitting, since the yielding process and the consequent departure from a linear response have already started when the storage modulus equals the loss modulus.[82] Additionally, the crossover between G' and G'' lies outside the linear region, thus the viscoelastic moduli only represent the fundamental harmonic of the oscillatory response.[80] Corker *et al.*[36] distinguished two different characteristic values of stress in the oscillatory response of GO pastes: the yield stress and the flow stress. Their ratio gives an indication of the brittleness of the ink and can be related to ink printability. The three-interval thixotropy tests (3ITT) are an easy way to study the thixotropy of inks,[83] however they have been rarely reported for energy materials. During 3ITTs, the ink is at first sheared at a low stress, to allow its microstructure to stabilize.[48] A high-stress interval follows, which destroys the microstructure of the ink, mimicking the flow inside the nozzle. Finally, during the last interval, a low shear stress is applied again, and the recovery kinetics of the material is measured. Extensional rheology has also been performed to assess printability, but extensional tests are often more complicated than shear rheology for yield stress fluids.[36]

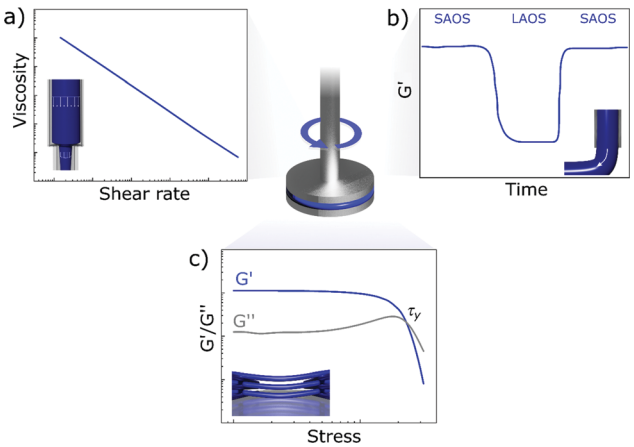

Fig. 6 Schematic showing the ideal rheological response of a printable ink, as determined through shear rheology: (a) flow curve showing a highly shear-thinning behaviour; (b) rapid recovery of the elastic modulus during 3ITT tests, after large amplitude oscillatory shear (LAOS); (c) solid-like behaviour below the yield stress.

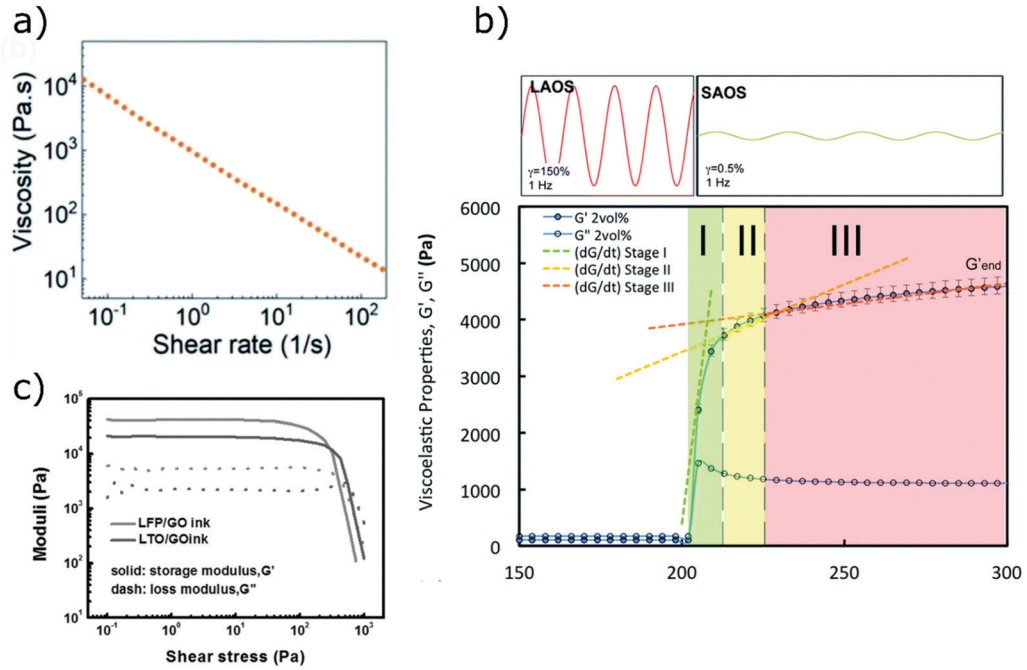

Fig. 7 Experimental data showing the ideal rheological behaviour of inks for DIW: (a) shear thinning flow behaviour (adapted with permission from ref. 149, Published by The Royal Society of Chemistry); (b) quick recovery of the storage modulus after large amplitude oscillatory shear (adapted with permission from ref. 36, published by The Royal Society of Chemistry 2019); (c) solid-like response below the yield stress (adapted with permission from ref. 92, Copyright 2016 John Wiley and Sons).

For example, in capillary break-up extensional tests, yield-stress fluids do not form cylindrical filaments and the filament thinning strongly depends on the initial deformation applied to the material.[84,85] The ideal rheological response of inks for DIW is presented in Fig. 6 and 7.[36,44,53]

Ink design

The fundamental components of an ink

Inks for 3D printing are often complex systems, made of different functional elements whose interaction must be carefully controlled. During ink formulation, two major objectives are pursued. Firstly, the ink must fulfil the rheological criteria discussed in the previous section in order to be printable. Secondly, the device that is obtained after solvent removal and post-processing should possess specific functional properties, such as high energy density, good electrical conductivity and mechanical integrity. These two aspects must be simultaneously taken into account for ink design, although they are often in contrast with one another. In fact, inactive and non-conductive species often need to be added to the active component to increase printability, hindering the electrochemical performance of the final device. These inactive species include stabilizers, surfactants and viscosifiers which must be subsequently removed at high temperatures, increasing the complexity and cost of the manufacturing process. High-temperature post-processing might also be detrimental for the properties of the electroactive material, causing decomposition or unwanted phase transitions. Nevertheless, electroactive materials that can also act as rheology modifiers have been recently proposed.[24,86] It is, for example, the case of graphene oxide, which can be used to form printable pastes at high concentration and also provides conductive paths and capacitive behaviour after thermal or chemical reduction. Therefore, in some cases the active functional materials can be also used to control rheology.

Another common categorization for ink components has been discussed by Hu *et al.*[87] and draws inspiration from typographic inks. Ink components are divided into functional fillers, binders, additives and solvents.[12,87,88] Functional fillers are responsible for the functional properties of the final device, and in the context of energy materials they can range from carbonaceous materials to ceramics and metals. Functional fillers are usually in the form of colloidal particles or nanomaterials, such as nanoflakes, nanotubes, nanowires and quantum dots. The use of nanomaterials is often twofold: they present unique electronic properties and they are several orders of magnitude smaller than the nozzle diameter, hence they avoid clogging.[89] Suspensions made of nanoparticles are also less prone to sedimentation and promote ink stability, which is important to avoid changes in rheology during printing.[90] In addition, nanoparticles can shorten transport pathways and minimize the volume variation during cycling of batteries.[91] Conductive fillers are particularly important in three-dimensional energy devices to promote electron transport through the electrode to the current collector.[92]

Binders are usually polymeric materials used to bind particles together and promote adhesion with the substrate. Examples of

inorganic or electroactive binders have also been proposed recently.[93,94] These materials have a role in controlling the stability of the inks and in preventing particle sedimentation. However, they often need to be removed after printing because they limit the electrochemical performance of the system. Therefore, the amount of binders added to the ink must be minimized, although this can sometimes lead to inhomogeneities in the ink affecting the final performance of the printed structure.[95] As an alternative, binders can also be converted into functional components after printing, *e.g. via* thermal carbonization or reduction.[76]

The solvent is a fundamental component of DIW inks, necessary to give fluidity to the system during the extrusion and the deposition processes. Organic solvents can be flammable, toxic or leave residues that hinder the electrochemical performance of the printed devices. Therefore, aqueous inks are usually preferred for their lower cost and greater sustainability. Finally, additives are supplementary ingredients that are included in the ink formulation to control specific properties, such as particle dispersion, drying rate or rheology.

The classification presented here will be used in the next section to discuss the composition of the inks for the DIW of energy devices.

Ink formulation strategies

A large number of ink formulations proposed for energy materials have been directly inspired from ceramic processing. Direct ink writing was in fact originally developed for the fabrication of dense ceramic structures and significant effort has been devoted to the study of ceramic inks in the past. Common goals can be identified between ceramic printing and energy device fabrication, which made it possible to apply techniques originally developed for ceramics to the broad class of energy materials. These include: (1) need for low amounts of binders and high fractions of active materials; (2) reduction of the nozzle diameter to achieve high printing resolution; (3) shape retention and mechanical integrity after printing and post-processing. Nevertheless, energy devices also require additional features that are not usually pursued in ceramics research, such as electrical conductivity and high specific surface area. Here we review the recent ink developments to meet these specific requirements. There are several ways in which inks for DIW can be categorized. In the following discussion they are classified on the basis of the type of solvent, binder and the interactions between the solid particles within the ink.

Inks based on organic solvents. Fluorinated polymers have been widely used to formulate slurries for the fabrication of commercial batteries, usually *via* coating processes.[96] In particular, polyvinylidene fluoride (PVDF) and its copolymers provide high mechanical and thermal stability and favourable electrochemical properties when used as binders.[97] However, PVDF is usually dissolved in organic solvents, since it presents low solubility in water. Recently, inks for DIW based on fluorinated polymers and organic solvent have been proposed.[57,98] Kohlmeyer *et al.*[98] used PVDF as a binder to obtain printable inks from $Li_4Ti_5O_{12}$ and carbon nanofibers dispersed in *N*-methyl-2-pyrrolidone (NMP). $Li_4Ti_5O_{12}$ acted as the active material for Li-ion batteries, while carbon nanofibers provided a conductive network to promote electron transport across the electrode. Although the use of carbon nanofibers prevented cracking during curing, they were also responsible for a shear-thickening behaviour observed at high shear rates, which deters the extrudability of the inks. The use of different active materials ($LiFePO_4$ and $LiCoO_2$) did not alter the rheology of the inks. However, the electrodes consisted of a single printed layer, which ultimately provided thin structures of 100–200 μm in height.

All-fibre Li-ion batteries with potential applications in wearable electronics can also be fabricated through DIW, as demonstrated by Wang *et al.*[57] They formulated inks with a composition similar to industrial slurries for Li-ion batteries,[96] consisting of active material particles (either LTO or LFP), PVDF-*co*-HFP and carbon nanotubes. The formulation was optimized to present higher yield stress and storage modulus than conventional slurries, in order to enhance printability. Single fibres were printed in an ethanol coagulation bath, and then soaked in a gel electrolyte and twisted together to form a 1D battery. The polymeric binder gave flexibility and mechanical strength to the fibre electrodes, allowing their integration into textile.

As organic solvents can be toxic or flammable, and they pose environmental problems and safety issues in large-scale production systems,[99] recent research on ink formulations has predominantly centred on aqueous systems. To this end, hydrophilic materials able to form hydrogels have been often considered.[65,75,99]

GO and MXenes: towards binder-free inks. Printed electronics would greatly benefit from inks containing minimal amounts of inactive binders to enhance their performance and environmental sustainability, and to reduce the cost of the manufacturing process. So far, two main ink formulations have been developed for DIW which do not rely on binders to attain printability. They are based on aqueous dispersions of highly hydrophilic atomically-thin materials with high aspect ratio (lateral sizes up to ~50 microns), namely graphene oxide (GO) and MXenes (Table 1).

GO is a derivative of graphene that presents oxygen-containing functionalities (hydroxyl, epoxy and carboxyl groups) along the basal planes and edges of the honeycomb carbon structure.[100–103] These functional groups make graphene oxide highly dispersible in water, even at very high concentrations.[104] The influence of GO concentration on the rheology of water suspensions was studied by Naficy *et al.*,[105] who showed that a gel behaviour starts appearing over a critical threshold (~2.5 mg mL^{-1}). The storage modulus and the yield stress grow with the concentration and are dependent on the lateral size of the GO flakes. These rheological features arise from the formation of hydrogen bonds between the oxygen-containing moieties on GO sheets and water molecules,[106–108] and can be exploited to formulate printable inks without any binders (Fig. 8d). For example, García-Tuñón *et al.*[106] showed that water dispersions containing up to 3.5 vol% GO flakes with large lateral dimensions (~44 μm) can be printed through direct ink writing without the need of additional rheology modifiers. These inks exhibit a storage modulus of ~10^5 Pa which is quickly recovered after shear and allows the fabrication of complex architectures (Fig. 8a–c).

Table 1 Comparison between MXenes- and GO-based inks for direct ink writing

Material	Aspect ratio	Concentration	Conductivity	Post-processing	τ_y and G'	Ref.
$Ti_3C_2T_x$	1–2 μm *vs.* 2 nm	36 mg mL^{-1}	2000 Ω sq^{-1} (1 line) 10 Ω sq^{-1} (5 lines)	None		24
$Ti_3C_2T_x$	8 μm *vs.* 1–3 nm (aspect ratio ~4000)	50 mg mL^{-1}		Freeze-drying	τ_y = 206 Pa G' = 36 507 Pa	73
N-Doped $Ti_3C_2T_x$ + GO + AC + CNTs				Freeze-drying + reduction in HI	τ_y = 300 Pa G' = 2 × 10^5 Pa	122
$Ti_3C_2T_x$	0.3 μm (lateral size)	290 mg mL^{-1}		None	τ_y = 24 Pa G' = 2 × 10^4 Pa	65
GO		20 mg mL^{-1}	170 S m^{-1}	Freeze drying + reduction in HI	τ_y = 50 Pa G' = 3 × 10^3 Pa	109
Holey GO	>1 μm *vs.* 2 nm	100 mg mL^{-1}		Freeze-drying + thermal reduction @1000 °C in Ar	τ_y = 500 Pa G' = 3 × 10^4 Pa	81
GO + Ca^{2+}	5–20 μm (lateral size)	20 mg mL^{-1}	800 S m^{-1} after thermal treatment @3000 K	Freeze-drying + reduction in HI or thermal treatment	τ_y = 160 Pa G' = 6 × 10^4 Pa	74
GO + Pluronic F-127 + HPMC		40 mg mL^{-1} (initial GO suspension)		Polymer curing @85 °C + freeze-drying + annealing at 1050 °C in N_2 + growth of PPy	τ_y = 60 Pa G' = 1 × 10^5 Pa	52
GO + urea + GδL	0.6–1.2 μm *vs.* 1 nm		40 S m^{-1}	Freeze-drying + reduction in HI @120 °C	GO solutions: τ_y = 40 Pa G' = 1 × 10^3 Pa GO inks: τ_y = 450 Pa G' = 4 × 10^4 Pa	51
GO in water + PANI in NMP		16 mg mL^{-1}		Reduction in HI	GO solution: τ_y = 90 Pa G' = 2 × 10^3 Pa	125
GO scaffold		120 mg mL^{-1}		Annealing in Ar/H_2 at 700 °C	τ_y = 40 Pa G' = 3 × 10^5 Pa	5
GO + silica + gelling agent	150–400 nm (lateral dimensions of single layers)	20–40 mg mL^{-1}	87 S m^{-1} (20 mg mL^{-1}) 198 S m^{-1} (40 mg mL^{-1})	Curing at 85 °C + supercritical drying in CO_2 + annealing at 1050 °C in N_2 + etching in HF	20 mg mL^{-1}: τ_y = 35 Pa G' = 8 × 10^2 Pa 40 mg mL^{-1}: τ_y = 100 Pa G' = 6 × 10^3 Pa	113

Binder-free inks based on GO were originally proposed for advanced ceramics, but have been readily applied to the fabrication of batteries[81] and supercapacitors.[74,109] Woodpile structures were for example fabricated by Jiang *et al.*[74] and tested as electrodes for supercapacitors after reduction in a hydroiodic acid solution. The chemical or thermal reduction of GO structures after printing is necessary to repristinate some electrical conductivity (up to 0.4 S cm^{-1} for printed filaments presenting a density of 6 mg cm^{-3})[110] and favour electron transfer to the current collector. Before the reduction process, printed GO electrodes are usually freeze-dried to completely remove water and increase the surface area accessible to the electrolyte ions. Li *et al.*[109] showed that it is possible to control the structure of GO electrodes from a macroscopic to a microscopic scale using a combination of DIW and freeze-drying at different temperatures. They fabricated supercapacitors with optimized porosity and high mechanical flexibility, displaying a 97% capacitance retention over 200 bending cycles. A further degree of control was achieved by Lacey *et al.*,[81] who employed holey GO flakes to introduce nanopores in the electrodes. The structures printed from concentrated inks (~100 mg mL^{-1} of holey GO) presented trimodal porosity, which ensured promising electrochemical performance for Li–O_2 battery cathode.

Binder-free GO inks have attracted great attention for their numerous advantages. Firstly, GO inks are water-based and do not require toxic or flammable solvents to improve colloidal stability. Secondly, the ink composition is simple and scalable, and the porosity of printed GO can be easily controlled with freeze-drying. However, high volume fractions of GO are usually necessary to obtain printable pastes, implying time-consuming procedures for concentration and redispersion.[74] Post-processing after printing is necessary to make the structure electrically conductive, although the conductivity of reduced GO is significantly lower than graphene conductivity, owing to its inherently defective structure.[101,111]

Physical and chemical crosslinking are viable routes to increase the connectivity of GO sheets in aqueous inks.[112] In this way, it is not only possible to enhance the ink printability but also to increase the electrical conductivity[113] and the mechanical strength[114] of the GO architectures. For example, small amounts of Ca^{2+} ions can be added to GO suspensions to form coordination bonds with the carboxyl and hydroxyl moieties and bridge different flakes. It is thereby possible to control the rheology of inks and improve printability without altering the concentration of GO. The storage modulus and yield stress of GO inks (8–20 mg mL^{-1} of GO) can be increased of one order of magnitude with the addition of $CaCl_2$ (15 mM), as demonstrated by Jiang *et al.*[74] (Fig. 8e and f). This approach shows strong similarities with the ionic gelation of functionalized ceramic particles induced by multivalent cations, which has been widely investigated to formulate inks for robocasting.[44] Urea has also been used to induce a moderate crosslinking of

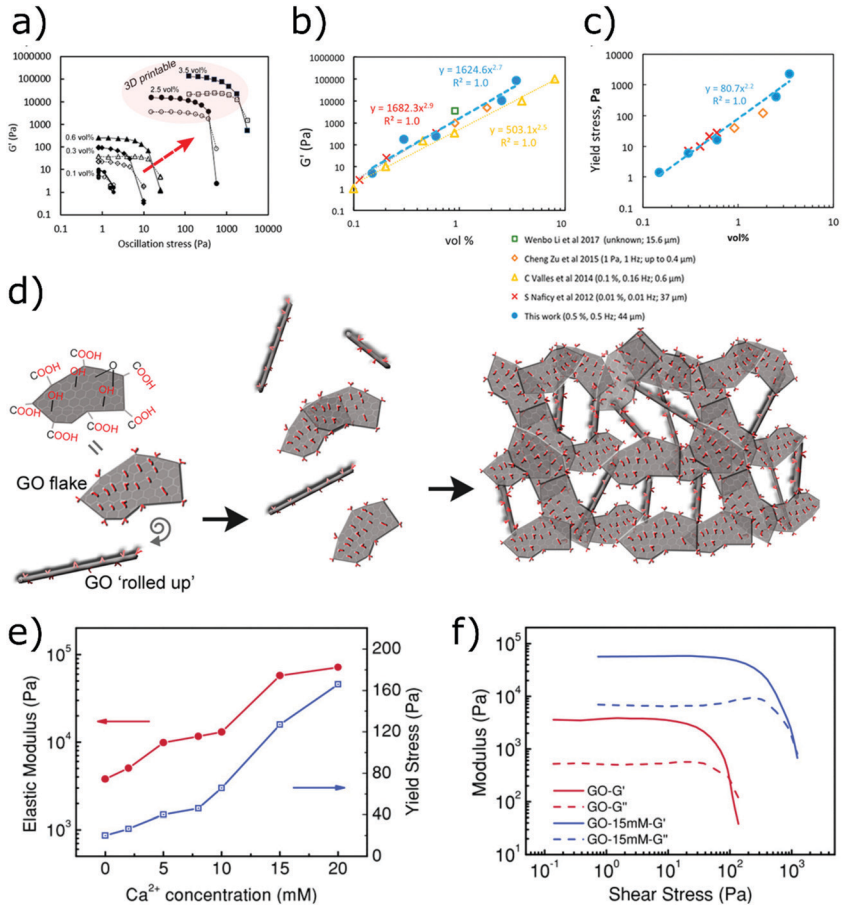

Fig. 8 (a–c) Viscoelastic moduli and yield stress of GO dispersions at different concentrations (adapted with permission from ref. 106, Copyright 2017 American Chemical Society); (d) self-assembly of GO flakes in water mediated by the oxygen-containing moieties on their surface (adapted with permission from ref. 106, Copyright 2017 American Chemical Society); (e and f) viscoelastic moduli of GO suspensions physically cross-linked with Ca^{2+} cations, at different cationic concentrations (adapted with permission from ref. 74, Copyright 2018 John Wiley and Sons)

GO sheets through the release of ammonium ions, which promotes the formation of hydrogen bonds.[51] The hydrogen bonds between ammonium ions and GO sheets increase the elasticity and strength of the gel by over and order of magnitude.[51] Alternatively, resorcinol and formaldehyde can be added to the GO ink to form covalent bonds through sol–gel chemistry, usually in the presence of sodium carbonate as a catalyst. Chemical gelation is subsequently induced with a thermal treatment after printing, and the crosslinked structure can then be reduced in inert atmosphere. This process was shown to increase the mechanical recovery after compression and the rigidity of the printed GO scaffolds, although it involved temperatures over 1000 °C.[113] Additionally, this approach allows the control the surface area, density and conductivity of GO structures by simply altering the concentration of resorcinol and formaldehyde. Graphene nanoplatelets (GNP) can then be added to the cross-linkable GO inks to increase the electrical conductivity of almost one order of magnitude and enhance the capacitive performance, while retaining high specific surface area.[115]

High aspect ratio GO sheets can be used to enhance the rheological properties of the inks and the conductivity of the annealed structures. In particular, flakes with larger lateral dimensions result in lower gelation concentrations and fewer inter-sheet junctions, reducing the contact resistance.[116,117] However, the graphene oxide used in DIW is usually obtained through the modified Hummers' method for the oxidation of the graphite platelets, and large crystals would significantly slow the reaction kinetics during this process.[118] For this reason, instead of trying to use large graphene oxide flakes, polymeric binders and rheology modifiers are often used to improve printability, however increasing the complexity of the system.[6,52,75,115] Common binders are hydroxypropyl methylcellulose (HPCM), Pluronic F-127 and silica, which can enhance the viscosity of GO inks by several orders of magnitude.[6,52,75,115] Silica and Pluronic F-127 can also act as template agents to increase mesoporosity upon removal *via* thermal treatment or chemical etching.[52,115]

In summary, GO has attracted great attention for its ability to form printable inks in water without the addition of binders or additives. However, despite their simplicity, inks based on graphene oxide have a limited electrical conductivity, thus chemical reduction steps at temperatures higher than 1000 °C are needed to fabricate conductive structures for energy storage. After reduction, GO exhibits a capacitive behaviour, confining its use to supercapacitors. Nonetheless, graphene oxide is versatile

material since it can be also used as a rheology modifier to formulate inks based on a wide range of electroactive materials, as will be discussed in the next section.

Similarly to graphene oxide, MXenes present a two-dimensional atomically thin nature with negative surface charges and hydrophilic surface functionalities (–F, –OH and =O).[119] Additionally they are highly conductive, with a metal-like conductivity that reaches 6.5×10^3 S cm^{-1} for spin cast films,[120] making them particularly suitable for energy storage applications. Concentrated dispersions of MXenes in water are characterized by a volume spanning percolating networks of interacting particles, as discussed by Akuzum *et al.*[121] who have investigated the rheology of MXenes suspensions at different volume fractions (Fig. 9b). In particular, they showed that pastes containing high concentrations of monolayer $Ti_3C_2T_x$ (>1.80 mg mL^{-1}) have a suitable rheology for extrusion printing: G'/G'' ratio higher than ~2 and gel-like behaviour. However, their conclusions were mainly based on the viscoelastic response of MXene inks at low amplitudes (*i.e.* below the yield stress),[121] and overlooked other parameters that might be relevant for processing, such as yield stress and recovery time in the case of DIW.

The favourable pseudocapacitive behaviour and high electrical conductivity presented by MXenes are well suited for electrochemical applications.[122] As post-printing high temperature processes are not needed by inks based on MXenes, they are also compatible with flexible substrates, such as paper or plastic. Zhang *et al.*[24] have employed paper substrates to fabricate printed supercapacitors starting from aqueous $Ti_3C_2T_x$ inks (Fig. 10b). Their devices showed pseudocapacitive behaviour and good adhesion between flakes thanks to strong hydrogen bonds. Despite the high conductivity of the MXene thin films, the electron transport strongly depends on the orientation of sheets in the three-dimensional printed structures. Orangi *et al.*[65] showed that the printing process induces an alignment of MXenes in the direction of the nozzle movement, which determines a lower out-of-plane conductivity and slower charge–discharge kinetics in thicker structures.

As already discussed for graphene oxide, the morphology of MXenes platelets influences the rheology of the dispersion and it can be tailored to optimize printability. The use of platelets with high aspect ratio permits to achieve high viscosity at relatively lower concentrations (tens of mg mL^{-1} *vs.* thousands of mg mL^{-1}),[73] as demonstrated by Yang *et al.*[73] The inks they formulated consisted of $Ti_3C_2T_x$ sheets with large lateral size (~8 μm) and low thickness (1–3 nm), having an aspect ratio as high as ~4000.[73] The excellent printability of these inks was confirmed by rheological analysis (Fig. 9a), showing high storage modulus (~3.5×10^4 Pa) and quick structural recovery at a concentration of 2D platelets as low as 50 mg mL^{-1}. Printed architectures obtained from these high-aspect-ratio inks are presented in Fig. 10a.

The electrochemical performance of printed MXenes can be tuned through elemental doping achieved as a post-printing process. Yu *et al.*[122] used melamine formaldehyde spheres to

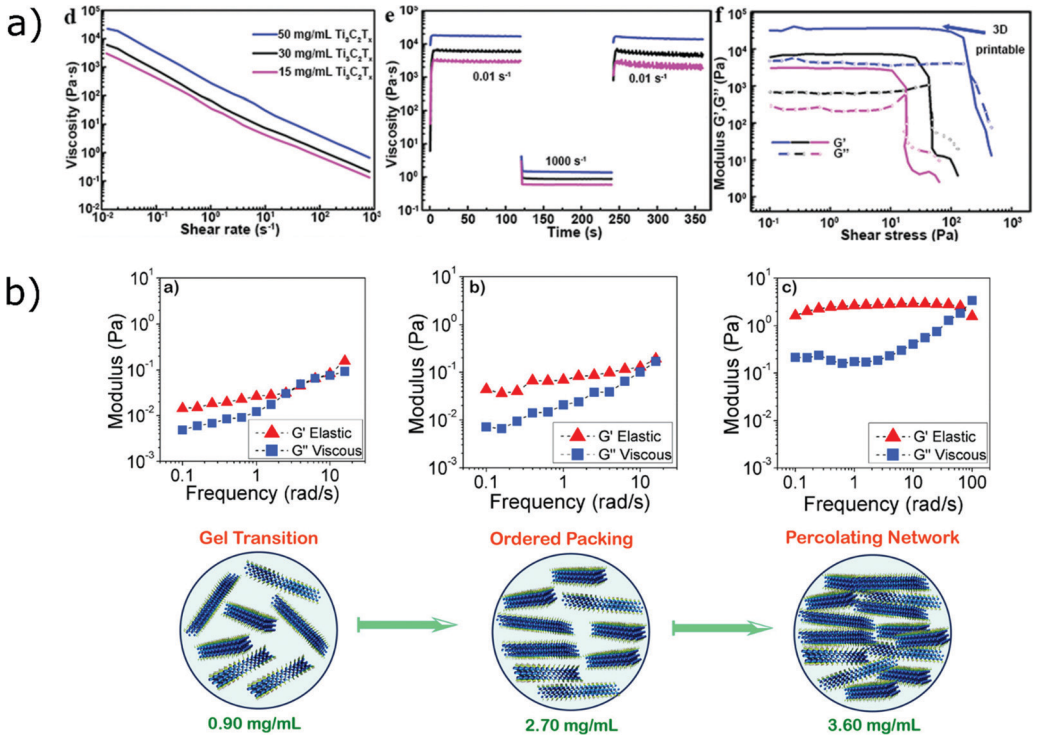

Fig. 9 (a) Shear rheology of $Ti_3C_2T_x$ dispersions at different concentrations: flow ramps showing shear-thinning, viscosity drop and recovery after shear at high rates and viscoelastic moduli of the suspensions (left to right, adapted with permission from ref. 73, Copyright 2019 John Wiley and Sons); (b) formation of a percolated network at increasing concentrations in MXenes suspensions (adapted with permission from ref. 121, Copyright 2018 American Chemical Society).

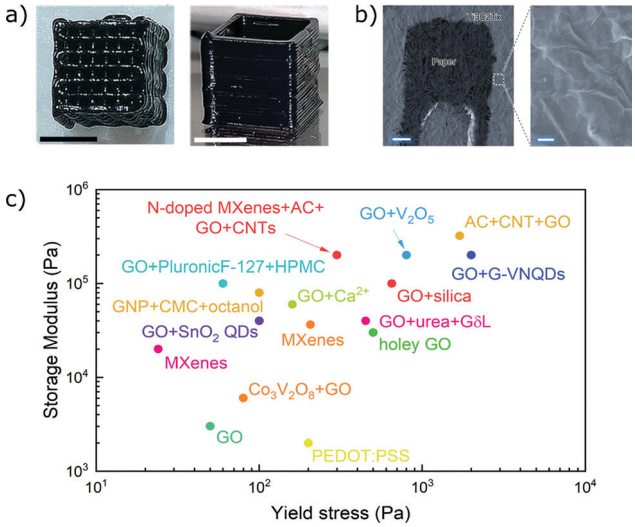

Fig. 10 (a and b) Pictures of structures printed from $Ti_3C_2T_x$ inks (adapted with permission from ref. 73, Copyright 2019 John Wiley and Sons, and from ref. 24, Copyright 2019 Springer Nature); (c) plot comparing the storage modulus and yield stress of DIW inks based on graphene oxide and MXenes (references in Table 1).

limit sheet restacking and induce nitrogen doping in the MXenes platelets after annealing the 3D printed structures in Ar. The N-doped sheets were then used to print supercapacitors on a variety of substrates (plastic, paper and metals).[122]

MXene-based inks present numerous promising features, such as high conductivity, favourable electrochemical properties and high hydrophilicity. MXene-based devices can be directly printed onto flexible substrates, since they do not require annealing or harsh post-processing steps. However, very high concentrations of flakes ($\sim$10–100 mg mL^{-1} to have $G' > 10^4$ Pa, depending on aspect ratio) are required to achieve printability, as already discussed for graphene oxide. The evaporation of water from MXenes suspensions to obtain concentrated inks is not only time-consuming, but it can also lead to the oxidation of the sheets if the temperature is increased to accelerate the process. The use of superabsorbent polymer beads has been reported as a faster route to concentrate $Ti_3C_2T_x$ inks without increasing the temperature to induce water evaporation.[65] However, even at room temperature $Ti_3C_2T_x$ platelets have low stability in water and in air and they can oxidize, showing a complete conversion to anatase titania in around two weeks,[123] which represents a significant limitation for water-based inks. The scalability and the safety of the ink preparation is also a concern. The current synthesis route of MXenes heavily relies on highly toxic hydrofluoric acid to etch and exfoliate the parent MAX phase.[119] Finally, $Ti_3C_2T_x$ is the only MXene employed so far in inks for DIW, and its applications have been limited to printed supercapacitors, whereas the family of MXene currently comprises almost 30 compounds, representing a promising field in the future.[124] It is clear that MXene-based inks have just started to be investigated, and their potential is yet to be fully explored. The properties of DIW inks based on GO and MXenes are summarized in Fig. 10c and in Table 1.

GO-Based multifunctional inks. Reduced graphene oxide electrodes usually present a capacitive behaviour dominated by electric-double layer (EDL) processes,[109] even though broad redox peaks have been observed in some instances.[74] GO electrodes are therefore mainly employed in EDL supercapacitors.[5] In order to enhance the capacitive behaviour and extend the application of GO to other electrochemical devices, particles of different electroactive materials have been blended with the graphene oxide slurries to prepare GO-based multifunctional inks. In these systems, GO acts as a co-functional material, binder, rheology modifier and scaffolding element (Fig. 11).

Shen *et al.*[86] used this approach to produce 3D printed cathodes for Li–S batteries. Notably, the addition of sublimed sulfur to the GO paste did not significantly alter the rheological properties of the dispersion (viscosity and viscoelastic moduli), suggesting that the printability of GO-based inks relies entirely on the attractive network of GO platelets. The electroactive materials added to the GO paste are usually in the form of nanoparticles or nanosheets to prevent clogging and increase the electrical conductivity of the network or fulfil other functional properties.[91,126] ZnV_2O_6@$Co_3V_2O_8$ and VN with sheet-like structure were added GO slurries by Zhao *et al.*[127] to produce electrodes with pseudocapacitive charge storage mechanism and to increase the electrochemical performance of pure reduced-GO scaffolds. Nanoparticles can also prevent restacking and enhance the surface area of the graphene structure, as noticed by Tang *et al.*,[4] who used $Ni_{0.33}Co_{0.66}S_2$/GO inks to fabricate nature-inspired hybrid energy storage devices. All carbon-based supercapacitors have been demonstrated by Gao at al.,[61] mixing GO, activated carbon and carbon nanotubes, while Tang *et al.*[51] showed the possibility to print mixed-dimensionality aerogels which combine 2D graphene oxide with Ag nanoparticles (0D), multiwalled carbon nanotubes (1D) or MoS_2 nanosheets (2D).

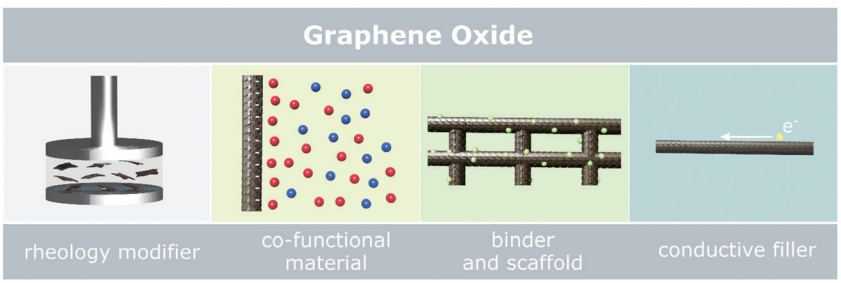

Fig. 11 Schematics showing the functions fulfilled by graphene oxide in DIW inks.

GO-Based formulations made it possible to print conductive polymers, that usually do not present a suitable rheology for DIW. Conductive polymers can be dissolved in an organic phase (such as NMP) and then mixed with a GO water-based suspension to obtain a printable paste.[125] Polymers like polyaniline can easily self-assemble on GO sheets thanks to π–π interactions and improve the stability of the network.[125] Otherwise, the use of organic solvents can be avoided by directly growing the conductive polymer onto graphene oxide sheets, as demonstrated by Liu *et al.*[99] (Fig. 12b). Polyaniline was at first grown on GO through interfacial polymerization. After this process, graphene oxide was not stable in water anymore since the hydrophilic moieties were covered by polyaniline. PEDOT:PSS was then added to improve the colloidal stability of the suspension and allow printing. However, the yield stress of the ink was not sufficient to print structures with good resolution on hydrophilic substrates, and lateral spread of the ink filaments was observed.[99]

To prevent the active material from inducing significant alterations in the printability of GO pastes, it can be deposited onto the GO scaffold after printing, for example *via* chemical deposition.[5,6,51,52,128] GO scaffolds offer high mechanical flexibility and structural integrity, and have shown great compressibility with complete recovery after large deformations.[113] Highly compressible electrodes were fabricated, for example, by Qi *et al.*[52] *via* chemical deposition of polypyrrole onto printed GO structures. The electrodeposition of the active material onto printed scaffold is also possible, as demonstrated by Yao *et al.*[129] They have electrodeposited MnO_2 nanosheets and VO_x nanowires on 3D printed graphene oxide to fabricate symmetric and asymmetric supercapacitors. The main advantages of this fabrication process is the possibility to finely control the composition and the amount of pseudocapacitive materials deposited onto the GO scaffold, as highlighted by Wang *et al.*,[5] who electrodeposited MnO_2 and Ni–Co–O nanosheets with tuneable Ni/Co ratio to fabricate asymmetric supercapacitors (Fig. 12a). In contrast, thermal shock was used by Qiao *et al.*[128] to decompose $NiCl_2$ deposited on reduced graphene oxide scaffolds to form Ni particles. The printed scaffold loaded with Ni particles was then used as a cathode for Li–CO_2 batteries. A pseudocapacitive behaviour can also be induced in printed GO scaffold *via* chemical functionalization. Yao *et al.*[6] electrochemically oxidized r-GO structures in KNO_3 to increase the oxygen-containing functional groups through a controllable process. The electrodes were reduced in hydrazine hydrate to improve their conductivity. After this treatment, the 3D electrodes showed a substantial increase in capacitance arising from the pseudocapacitive processes induced by the new functional groups.

Multifunctional inks based on graphene oxide are extremely versatile and GO can almost be considered a universal binder,

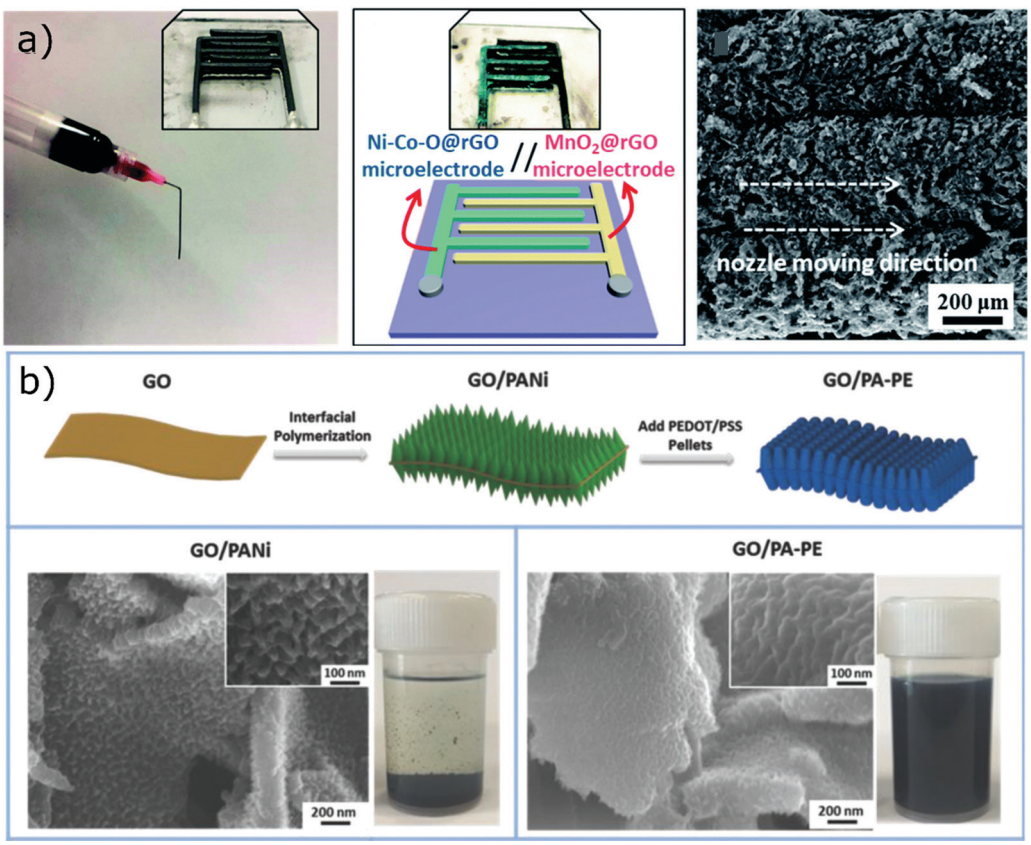

Fig. 12 (a) Growth of active materials on printed GO scaffolds to fabricate asymmetric supercapacitors (adapted with permission from ref. 5, Published by the Royal Society of Chemistry), (b) growth of PANi onto GO flakes and addition of PEDOT:PSS as a surfactant to obtain printable inks; SEM pictures of the functionalized flakes (adapted with permission from ref. 99, Copyright 2018 John Wiley and Sons).

expanding the portfolio of materials that can be printed through direct ink writing. GO has also excellent scaffolding properties and it can reduce transport limitations forming porous and conductive structures that support the particles of electroactive materials. However, the final reduction step that is necessary to obtain conductive scaffolds can induce modification in the active material.[86] Even after thermal or chemical reduction, the conductivity of the structure can still be an issue, and the rate performance often shows a drop when increasing the number of printed layers as a consequence of slow kinetics.[91]

Inks based on polymeric binders. Polymeric binders have been widely used in the 3D printing of ceramic particles and are now receiving great attention for the fabrication of biomaterials. The low cost, environmental-friendliness and favourable rheological properties of some polymers, such as cellulose and its derivatives, have also attracted interests for printed energy devices, although they usually need to be decomposed or carbonized after printing.

Carboxymethyl cellulose (CMC) has been investigated as a potential substitute for PVDF binder in non-printed batteries. The numerous carboxymethyl groups on CMC molecules can efficiently link the particles of active material together and confer high viscosity and shear-thinning behaviour to aqueous slurries.[130] Zhou *et al.*[131] formulated CMC-based inks containing lithium iron phosphate and lithium titanate particles that were respectively used to print the cathode and the anode of Li-ion batteries. CMC was used to bind the particles of active materials and to control printability, whereas the addition of carbon nanotubes to the inks provided a percolating network for electron transport, increasing the conductivity of the insulating polymeric matrix. Silver nanowires have also been used to increase the conductivity of CMC inks for Li-ion batteries,[132] although the rheological investigation was limited to the evaluation of the shear-thinning exponent and the inks did not exhibit good shape retention.

The amount of insulating polymer must be carefully optimized to enable printability without limiting the electrochemical rate performance. To this end, Drews *et al.*[133] studied the effect that the amount of binder (CMC and styrene–butadiene rubber) has on the printability of inks and on capacity retention at high rates. The optimal mass fraction for Li-ion microbatteries was found to be around 18 wt%, much higher than the binder content in industrial Si/C–graphite blend anodes ($\sim$6 wt%).[133]

Cellulose nanofibers (CNFs) are a type of nanocellulose with promising applications in printed electronics.[134] CNFs are rich in hydroxyl groups that promote the formation of hydrogen bonds between fibrils and water molecules and give mechanical strength after drying. CNF hydrogels can be directly loaded with the particles of active material to formulate printable inks. Cao *et al.*[76] used CNFs–$LiFePO_4$ inks to print cathodes for Li–metal batteries without the use of conductive fillers.[76] After printing, the electrodes were freeze-dried and annealed at 700 °C in order to carbonize the polymer. The carbonized nanocellulose fibres provided a conductive scaffold to support LFP particles, presenting good connectivity and mechanical robustness. Interestingly, in the same study CNF inks were also used to fabricate the anode of Li–metal batteries. Pure CNFs electrodes were printed, freeze-dried and carbonized to obtain porous carbon structures, that were used as anode electrodes after lithium infusion. The porous scaffold was able to prevent Li dendrite growth, as experimentally observed and confirmed by first-principle calculations.[76]

Hyaluronic acid (HA) is a natural polymer like cellulose that can be used as binder and rheology modifier in inks for DIW. Bio-compatible inks based on carbon nanotubes and either hyaluronic acid or gelatin methacryloyl were formulated by Shin *et al.*[135] to realize electrochemical devices. The rheology of gelatin methacryloyl inks was not suitable to print 3D structures *via* DIW, because of the weak electrostatic interactions between the binder and the active material. Therefore, gelatin methacryloyl was replaced by hyaluronic acid, which presents higher charge density and was able to promote the gelation of the suspension, and the concentration of nanotubes was increased. Deoxyribonucleic acid (DNA) was also used as a natural and bio-compatible additive to disperse the nanotubes.

Another polymeric binder widely used in direct ink writing is Pluronic F-127. Pluronic F-127 is a triblock copolymer able to form thermoresponsive hydrogels at sufficiently high concentrations in water ($>$20 wt%).[136] Pluronic-based inks were originally developed for ceramic particles,[43] but this formulation has high versatility and can be easily applied to energy materials.[75] Lyu *et al.*[137] used Pluronic F-127 to formulate printable inks from Co-MOF. The poly(propylene oxide) block of Pluronic F-127 can adsorb onto Co-MOF particles contributing to their dispersion, while the poly(ethylene oxide) block protrude in water and form a reticulate network that supports the particles. The rheological analysis showed that the inks had solid-like character at rest but could flow when sheared over the yield point, causing a reversible breakdown of the weak bonds. After printing, the structures were carbonized and used as self-standing catalysts for Li–O_2 batteries.

The formulation of inks based on polymeric hydrogel is usually extremely easy and time-efficient, and numerous polymers are available to control the rheology of active materials for energy devices. However, polymeric inks for DIW usually rely on inactive polymers, since it is difficult to obtain extrudable pastes from aqueous dispersions of electroactive polymers, such as conductive polymers. Nevertheless, inks entirely based on PEDOT:PSS dispersions have been recently demonstrated by Yuk *et al.*[138] (Fig. 13). The inks were obtained *via* the lyophilization and re-dispersion of aqueous PEDOT:PSS solutions, in order to increase the concentration of PEDOT:PSS nanofibrils and obtain a paste-like rheology. At high polymer concentrations, the nanofibrils formed reversible networks *via* entanglement, that ultimately lead to physical gels with shear-thinning and shear-yielding behaviour.[138] PEDOT:PSS inks could be printed through extremely fine nozzles (30 μm in diameter) to fabricate conductive (155 S cm^{-1}) and flexible multi-electrode arrays.

Inks based on capillary suspensions. The term capillary suspensions was proposed by Koos *et al.*[139] to indicate suspensions that are characterized by a sample-spanning network of particles held together by capillary forces. In particular, to prepare capillary suspensions, a small amount of a secondary fluid immiscible with the primary fluid phase is introduced into the system, *e.g.* octanol

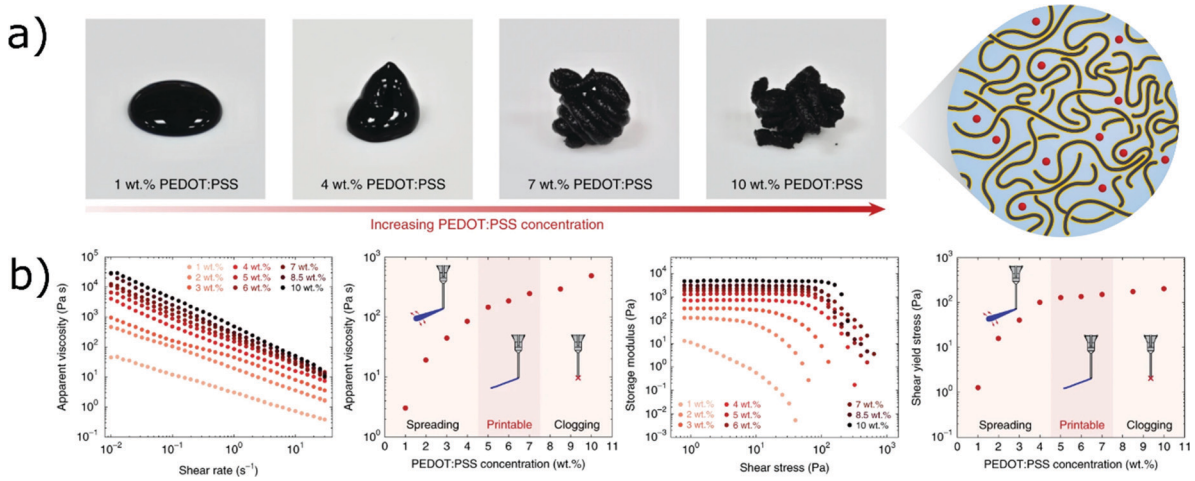

Fig. 13 (a) Images of the PEDTO:PSS inks at different polymer concentrations and schematic showing the network of entangled nanofibers in the inks; (b) rheology of PEDOT:PSS inks at different concentrations (all panels adapted with permission from ref. 138, Copyright 2020 Springer Nature).

can be added to aqueous suspensions. If the secondary fluid wets the solid better than the primary fluid, it forms concave bridges between solid particles.[140] Otherwise, no bridges are formed, but the particles would still aggregate to form tetrahedral or octahedral clusters.[140] In both cases, a reticulate network is formed determining a rheological transition to a gel state (Fig. 14c). The rheology of the capillary suspension can be finely tuned by changing the fraction of secondary fluids in order to achieve the highest printability, without adding surfactants.[140]

The formulation of capillary suspensions is similar to Pickering emulsions, in which the colloidal particles self-assemble at the interface between the two immiscible fluids. Pickering emulsions also exhibit rheological properties that are favourable for direct ink writing and have been used to formulate printable inks from ceramic particles.[141] However, in contrast to Pickering emulsions, capillary suspensions are preferentially formed at lower volume fractions of the secondary fluid, since they are promoted by pendular bridges smaller than the particle size. Therefore, aqueous inks can be formulated from capillary emulsions with extremely small amounts of secondary fluid, as small as 0.2 wt%. Schneider *et al.*[142] prepared shear-thinning capillary pastes based on nickel and silver particles suspended in a mixture of water and terpineol for potential applications in capacitors and fuel cells. The solvent and secondary fluid could be removed more easily than the binders of commercial pastes, which usually leave residues hampering the electrical conductivity.

Capillary inks have also allowed to print aqueous suspension of graphene nanoplatelets, which usually require large amount

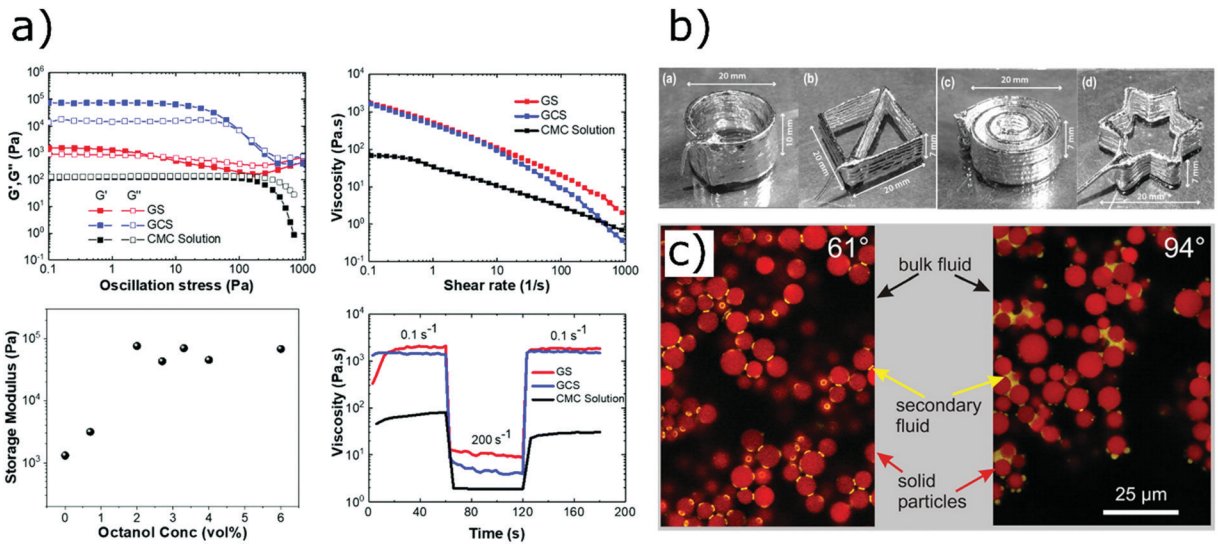

Fig. 14 (a) Rheological properties of capillary suspensions before and after the addition of the secondary fluid (adapted with permission from ref. 143, Published by The Royal Society of Chemistry); (b) 3D printed liquid metal inks (adapted with permission from ref. 144, Copyright 2018 John Wiley and Sons); (c) secondary fluid linking the solid particles of a capillary suspension (adapted with permission from ref. 140, Copyright 2016 American Chemical Society).

of binders to be stable, as reported by Ding *et al.*[143] Graphene nanoplatelets were dispersed in water with carboxymethyl cellulose to improve colloidal stability. Octanol (2 wt%) was then added to suspension to crosslink the nanoplatelets through capillary bridges. The storage modulus and the yield stress of the suspension increased of almost two orders of magnitude after the addition of octanol, indicating the formation of a strong and reversible network with favourable printability (Fig. 14a). Interestingly, the pastes containing octanol did not show a preferential orientation of platelets after extrusion, as revealed by X-ray tomography. Possibly, this is caused by the strong capillary bridges which reform after extrusion, causing a rotation of graphene platelets, thus destroying the order induced by the shear velocity. After heat treatment, the printed structures present high electrical conductivity (23.7 S cm^{-1}), promising for electronic applications.

The main advantage of capillary ink lies in the small amount of binder required, usually an organic solvent that can be easily removed through a heat treatment at temperatures lower than 350 °C. So far, this technique has only been explored for a very limited range of materials, although it holds potential for printed energy devices as it reduces possible contaminations which act as electrically insulating components.

Other ink formulations. The 3D printing of liquid metals, such as gallium alloys, has been recently explored for the fabrication of electronic devices. Although gallium alloys are low-viscosity liquids, when they are exposed to air a thin surface layer of oxide is formed, inducing a yield-stress behaviour. The moderate storage modulus and yield stress of pure Galinstan can be significantly improved by adding nickel particles and sonicating the suspension, as demonstrated by Daalkhaijav *et al.*[144] (Fig. 14b). The sonication process promoted the oxidation of Galinstan and the dispersion of the oxide layer into the bulk of the material, thus increasing the yield stress up to ~500 Pa and the storage modulus to ~15 kPa. The printed structure obtained from the Ni–Galinstan pastes presented a conductivity of 3.93×10^4 S cm^{-1}, showing that the sonication process did not have any relevant effect on the electrical properties of the material.

Other formulations used for energy devices include inks based on reactive precursors. For example, reactive inks were formulated by Chen *et al.*[54] to realize TiO_2 structures with controlled mesoporosity and high specific surface area (up to 259 m^2 g^{-1}) for artificial photosynthesis. A sol–gel precursor solution made of titanium diisopropoxide bis(acetylacetonate) (TIA) and dodecyl benzenesulfonic acid (DBSA) was concentrated by solvent evaporation to obtain a rheological behaviour suitable for printing (yield stress ~500 Pa and storage modulus ~10^4 Pa). SiO_2 particles were then added to the ink in small amounts as templating agent to increase porosity, without altering the printability of the paste. The inks were printed through 30 μm nozzles and annealed to convert the sol–gel precursor to anatase. Porous scaffolds were ultimately obtained after etching SiO_2 in KOH. The scaffolds were then functionalized with Au and RuO_2 to enable CO_2 electroreduction. These functionalized scaffolds were able to enhance CO_2 reduction more efficiently than powder catalysts in terms of reaction yield over time.[54]

Inks based on reactive precursors were also developed by Walker *et al.*[145] to fabricate conductive struts for electronics on flexible substrates, without the need of high-temperature post-processing to remove binders or convert the reactive precursors. The ink was formulated *via* a modified Tollens' process, which consisted in the dissolution of silver acetate in formic acid and ammonium hydroxide to reduce the silver ions and form silver particles. The silver particles were removed by sedimentation, whereas the supernatant, consisting of diammine-silver cations ($Ag(NH_3)_2^+$), acetate anions (CH_3COO^-) and formate anions ($HCOO^-$) was used as reactive ink. During the drying process the ammonia ligands evaporate and silver ions are reduced to metallic silver. Although the absence of silver particles in the ink allowed to extrude it through ultrafine nozzle (100 nm in diameter), there was significant spreading after deposition and the final strut width was around 5 μm, which was over an order of magnitude larger than the nozzle diameter. Interestingly, the printed struts showed a very high conductivity when compared to nanoparticle inks, equal to 10^4 S cm^{-1} after drying at 23 °C and to 6.25×10^5 S cm^{-1} after drying at 90 °C.

The use of reactive inks can facilitate extrusion, avoiding clogging caused by particles in the ink. However, shape retention after post-treatments might be a challenge, especially for three-dimensional structures with thickness of several millimetres.

Multimaterial fabrication of all-printed devices

Direct ink writing allows the deposition of different materials during the same printing process, making it possible to fabricate multimaterial systems and gradient architectures.[146,147] In particular, a single printing nozzle can be alternatively fed from different ink reservoirs to extrude filaments with different composition. Otherwise, a printing head with multiple nozzle can also be used.[148] The deposition of multiple materials in a single process is fundamental to fabricate all-printed energy devices, which rely on multiple functional components to operate.[39] Batteries and supercapacitors usually consist of a positive and a negative electrode, a current collector, an electrolyte and a protective case. As different rheological requirements and functional criteria should be met by the inks for the current collector, electrolyte and packaging when compared to the functional electrodes, we dedicate a separate section to those. Here we will discuss the designs of inks for these components and their integration into all-printed devices.

Printed current collectors

The role of the current collector is to gather the charges generated by the active material and convey them to the external circuit.[39] Current collectors should present good electrical conductivity, high contact area with the electrodes and small contact resistance in order to promote charge transfer. Additionally, the current collector should also be stable in the electrolyte within the widest potential window possible. To this end, metallic current collectors are generally used in energy devices. Metallic structures can be printed *via* DIW using dispersions of micro- or nanoparticles,

which are then sintered at high temperatures. As an example, a porous copper current collector was printed by Lim *et al.*[149] from inks containing copper particles and Pluronic F-127. Copper has been widely used as a current collector material for lithium batteries, presenting high stability, good electrical conductivity, and mechanical strength. However, the conductivity and the mechanical integrity of copper structures can be severely hampered if the polymer is not completely removed, leaving residues that prevent particle sintering. Therefore, Pluronic F-127 was at first decomposed with a thermal treatment in air, followed by a second thermal treatment in Ar/H_2 to reduce the metal particles. The copper scaffolds prevented dendrite growth in Li–metal batteries, increasing the life of the cell.

The shape of the current collector should match the geometry of the electrodes, without uncontrolled lateral spreading that might cause short-circuiting in interdigitated devices. Consequently, inks for current collectors should present high yield stress to prevent lateral collapse, but they should not be too stiff in order to promote good contact with the electrodes. Chae *et al.*[150] formulated inks based on Ni nanoparticle, Ni nanoflakes and polyvinylpyrrolidone (PVP), which presented a storage modulus almost two orders of magnitude lower than the carbon paste used to print the electrodes, and a high yield stress of $\sim$368 Pa. Interestingly, the nickel structures were simultaneously sintered and reduced in air through a flash-light sintering process mediated by PVP (Fig. 15). Under irradiation, the metal particles melted promoting the densification of the current collector, while the metal flakes helped limiting the volume contraction. The printed current collectors showed great stability in ionic liquid, with an operational potential window of 3 V.

Liquid metals such as gallium alloys can also be used to print current collectors, although they are more costly than copper or nickel.[144,150] Nonetheless, they have high conductivity (3.9×10^4 S cm^{-1}), stretchability and do not need binders or high post-processing temperatures. If the conductivity of the electrodes is sufficiently high, for example in the case of MXenes which present metallic conductivity,[73] the current collector is not necessary and the complexity of the manufacturing process can be then significantly reduced.

Printed electrolytes

In energy storage systems, the electrolyte ensures the transfer of ions between the electrodes and can act as a physical separator between them to impede short circuits (Fig. 17b).[13] The electrolyte should present high ionic conductivity, good wetting capability, and high contact area with the electrodes. McOwen *et al.*[90] showed that the ability of the electrolyte to conform to the electrodes can be tailored by adjusting the ink composition (Fig. 16). They developed two formulations, both based on garnet-type $Li_7La_3Zr_2O_{12}$ (LLZ): a conformal ink, with a Newtonian rheological behaviour, and a self-standing ink, presenting a yield stress. The Newtonian ink could be used to print thin and dense layers ($\sim$5–10 μm in thickness), presenting seamless joints between the printed lines; while the yield-stress ink was used to print thick structures with high aspect ratio and large surface area. A symmetric Li–metal cell was fabricated using the printed LLZ electrolytes, which ensured small transport resistance and superior performance.

The importance of good contact between electrodes and electrolyte was highlighted by Cheng *et al.*,[97] who used a high-temperature DIW process to print a polymeric electrolyte onto MnO_2 cathodes. The electrolyte ink consisted of poly(vinylidene fluoride-*co*-hexafluoropropylene) (PVDF-*co*-HFP) dissolved in NMP, to which TiO_2 was added to improve the printability and wettability of the ink. Surprisingly, higher concentrations of TiO_2 resulted in a reduction in viscosity, caused by a decrease in the entanglement density after the physisorption of the polymeric chains onto the ceramic particles. The high-temperature printing process promoted good contact between electrodes and electrolyte, leading to an improvement of the performance when compared to cast electrolytes.

Direct ink writing is usually employed to print solid state or gel electrolytes, since liquid electrolytes do not present a suitable rheology for printing. To overcome this limitation, it

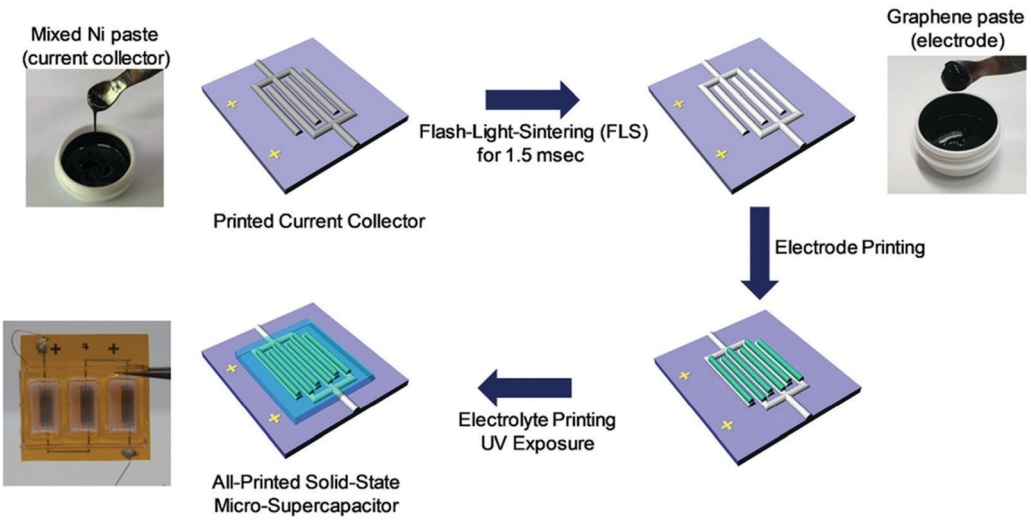

Fig. 15 Fabrication of Ni current collectors *via* a DIW and flash-light sintering process for graphene supercapacitors (adapted with permission from ref. 150, Copyright 2020 John Wiley and Sons).

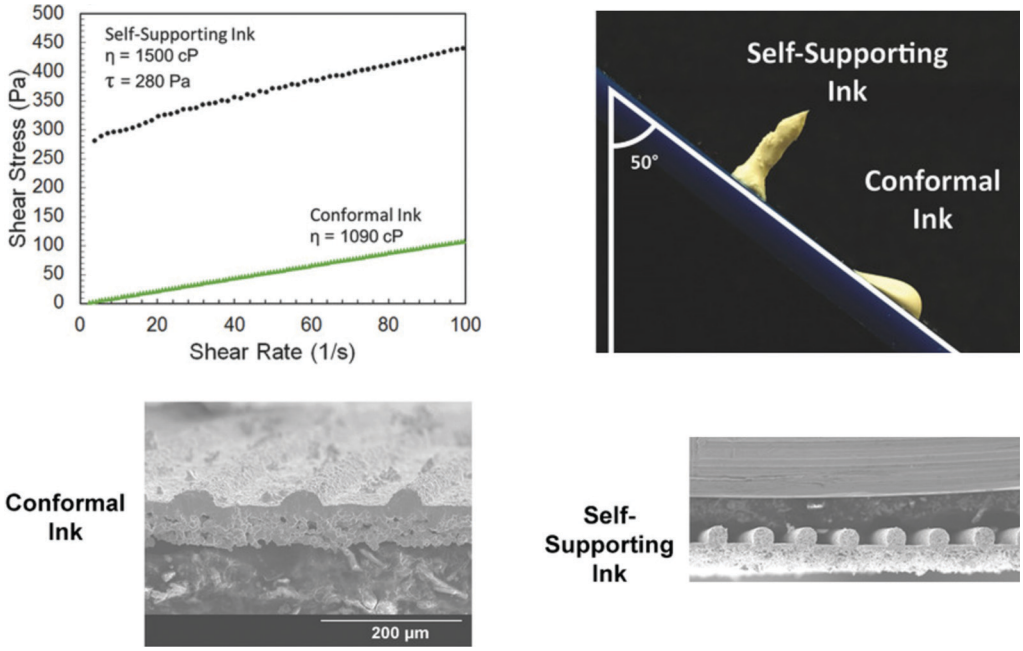

Fig. 16 Comparison between the self-supporting and conformal inks formulated by McOwen *et al.*[90] (adapted with permission from ref. 90, Copyright 2018 John Wiley and Sons).

is possible to fabricate a polymeric separator *via* DIW and then soak it with a liquid electrolyte, as demonstrated by Blake *et al.*[151] A phase inversion method was used to prepare the porous separators: PVDF was dissolved in a mixture of NMP (good solvent) and glycerol (weak nonsolvent). Al_2O_3 nanoparticles were then added to the mixture to control the pore size and increase the diffusion tortuosity to limit dendrite growth. The slurry could be directly printed onto a $LiFePO_4$ electrode to obtain a porous separator, that was subsequently soaked with liquid electrolyte ($LiPF_6$ in a mixture of ethylene carbonate and diethyl carbonate). The printing process promoted the diffusion of the electrolyte into the pore of the electrodes, improving interfacial contact.

Printed packaging

The cell packaging can also be realized through 3D printing, although very few studies have presented full cell cases printed with DIW. The packaging should be electrochemically inert, prevent the permeation of oxygen and moisture into the device and avoid leakage of the electrolyte.[13] Materials like ceramics (fumed silica) and curable polymers (epoxy resin) have been used to formulate inks for the cell packaging.[152] The packaging is usually fabricated by printing a conformal case around the electrodes and sealing it with a top layer after electrolyte casting. Generally, the complete case assembly is done once the device performance has already been optimized.

One of the challenges of packaging fabrication *via* DIW is to obtain devices with miniaturized footprint area, which requires printing the case as close to the electrodes as possible. The printed layers should perfectly merge and form a compact structure, to prevent electrolyte leakage and moisture penetration.

All-printed batteries

The possibility to integrate DIW into the fabrication of packaged batteries was demonstrated for the first time by Lewis' group.[53] In this study, water-based inks containing nanoparticles of active materials (LFP and LTO), cellulose binders and humectants (ethylene glycol and glycerol) were used to print Li-ion batteries. The miniaturized electrodes were deposited onto gold current collectors obtained with lithography and e-beam deposition (Fig. 17a). The electrodes were then packaged with laser-cut polymethyl methacrylate (PMMA) and sealed with PDMS. Finally, the liquid electrolyte was cast inside the PMMA case and the device was sealed with a glass cover. The polymeric case presented lateral dimensions that were significantly higher than the footprint of the electrodes (2.1 mm × 2.1 mm *vs.* 960 μm × 800 μm). While the electrode elements were realized *via* 3D printing, the full cell assembly required lithographic patterning, casting of the electrolyte and manual sealing of the packaging.

A step closer to all-printed Li-ion batteries was made by Fu *et al.*,[92] who formulated LTO and LFP inks based on graphene oxide for the electrodes and a PVDF-*co*-HFP ink containing Al_2O_3 particles for the electrolyte. The electrolyte viscosity and yield stress were adjusted to be significantly lower than the electrode inks, to promote wetting and filling of the pores during the printing process. Using GO instead of polymeric binders increased the conductivity of the electrodes and ensured slower water evaporation from the inks, as a result of the hydrophilicity of GO sheets. However, the battery casing was not realized through DIW and the cell had to be manually packaged using PDMS films in an Ar-filled glovebox.

A fully-printed Li-ion battery was presented in 2018 by Lewis' group.[152] Four different inks were formulated for the anode,

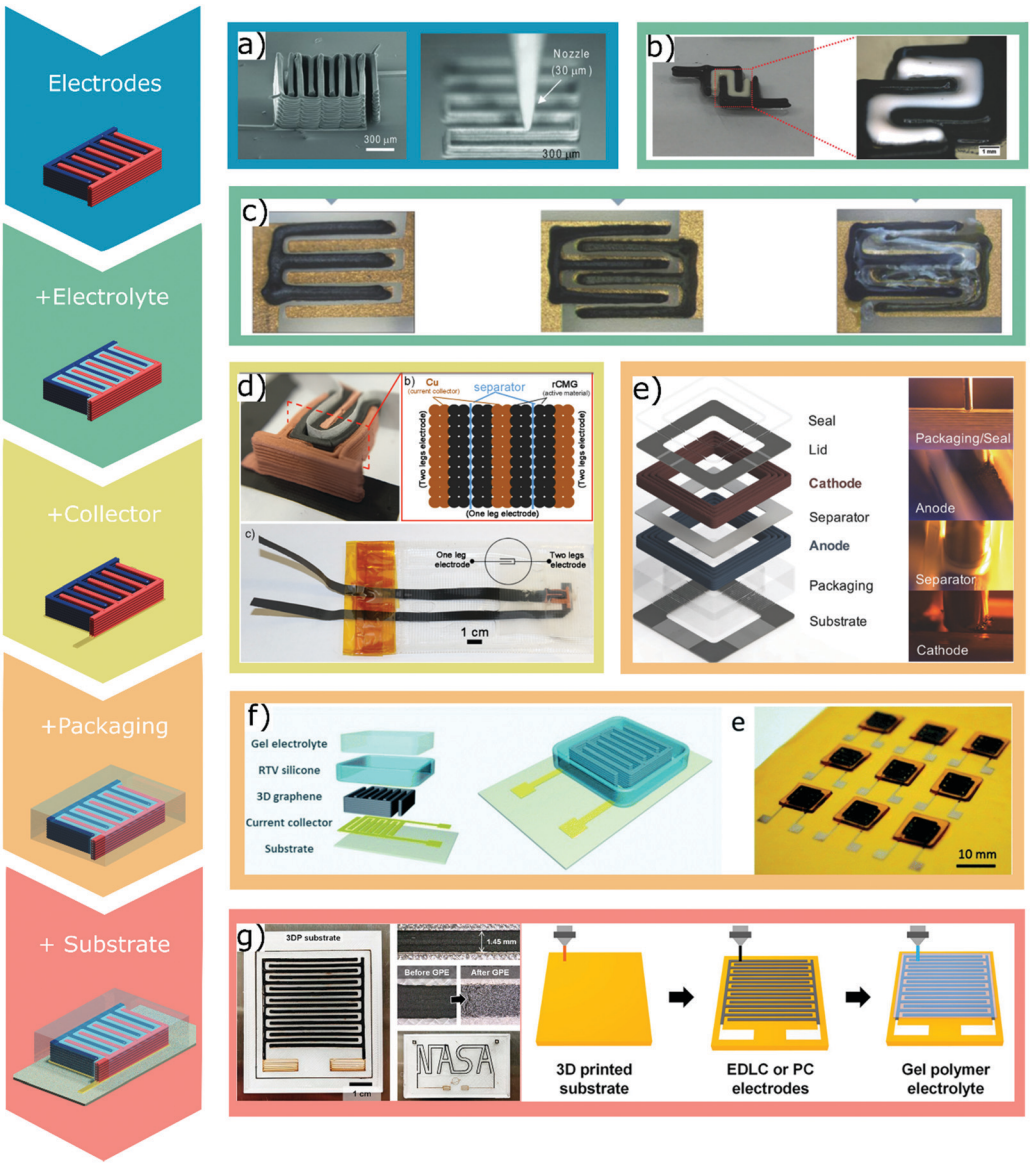

Fig. 17 3D printed components of batteries and supercapacitors fabricated *via* DIW: (a) printed electrodes (adapted with permission from ref. 53, Copyright 2013 John Wiley and Sons); (b and c) printed electrodes and electrolyte (adapted with permission from ref. 97, Copyright 2018 John Wiley and Sons, and ref. 153, Copyright 2018 John Wiley and Sons); (d) printed electrodes and current collector (adapted with permission from ref. 75, Copyright 2017 American Chemical Society); (e and f) printed electrodes, electrolyte, current collector and packaging (adapted with permission from ref. 152, Copyright 2018 John Wiley and Sons, and ref. 109, Published by The Royal Society of Chemistry); (g) all-printed device (adapted with permission from ref. 155, Copyright 2020 American Chemical Society).

cathode, separator and packaging (Fig. 17e). The electrode slurries were based on LFP, LTO and carbon black dispersed in an organic electrolyte (LiTFSI in PC) with PVP as a stabilizer. The same organic electrolyte was used for the separator ink, with the addition of Al_2O_3, a photocurable polymer and a photo initiator. In contrast, the packaging ink contained a mixture of SiO_2 and an UV-curable epoxy. The four inks were used to print a stacked battery presenting thick electrodes (~1 mm in thickness), which was finally capped with a layer of laser-cut glassy carbon as the current collector. Notably, the addition of a conductive filler in the electrodes (carbon black) was necessary to promote electric transport in thick structures and avoid the transport limitation presented by their previous battery,[53] resulting in superior performance.

Other full batteries obtained through DIW were recently reported by Cheng *et al.*[97] and Park *et al.*[132] The former printed LFP and LTO interdigitated electrodes using an ink based on PVDF and carbon black (Fig. 17b). A solid electrolyte ink was then deposited between the electrodes, and carbon paste was applied to realize the current collector. Finally, the device was sealed with PDMS gel. In contrast, Park *et al.*[132] used inks based on carboxymethyl cellulose and silver nanowires loaded with particles of active material (LFP and LTO, respectively) to print the electrodes of Li-ion batteries. The electrolyte ink was based on $LiClO_4$, polyethylene oxide and TiO_2 filler.

Although the research on printed electrodes is rapidly progressing, to date the studies on all-printed batteries fabricated *via* DIW have been focused on lithium-ion batteries based on LTO and LFP exclusively. This is a very promising approach for device fabrication and the ink formulations developed for the electrolyte and packaging of these devices could be adapted to newly emerging batteries, such as Na-ion, Li–S and Li–O_2 batteries.

All-printed supercapacitors

The fabrication of all-printed supercapacitors presents similar challenges as printed batteries. One of the most pressing challenge is to ensure low interface resistance between electrodes, electrolyte and current collector. The importance of good interfacial contact in printed supercapacitors was discussed by Rocha *et al.*,[75] who fabricated interdigitated devices consisting of GO electrodes and copper current collectors. Both inks were formulated using Pluronic F-127 as binder to promote the adhesion between the electrodes and the current collector during printing. Additionally, the composition of the copper ink was adjusted to match the volume contraction of GO electrodes during thermal reduction, in order to reduce the risk of delamination. The three-dimensional copper current collector was printed along the inner walls of the interdigitated electrodes, to further enhance the contact area with the thick GO structures (Fig. 17d). However, the electrolyte was not 3D printed, and the final device had to be manually assembled using a commercial cellulose separator and an ionic liquid electrolyte.

The DIW of both the electrodes and the electrolyte was demonstrated by Shen *et al.*[153] and Li *et al.*,[109] who fabricated interdigitated electrodes using graphene oxide inks (Fig. 17c). In both studies, the GO structures were printed onto metallic current collectors deposited *via* vacuum evaporation, then freeze dried and chemically reduced in hydrazine hydrate to obtain reduced graphene oxide.[154] The electrolyte inks (PVA–H_2SO_4 and PVA–LiCl in water, respectively) were subsequently deposited in the interspace between the electrodes. In Li's work the packaging was also realized *via* 3D printing, by depositing filaments of commercial silicone that was then cured for 24 h to obtain a square frame (Fig. 17f). Interestingly, the possibility to readily integrate the printed supercapacitors in an all-printed circuit was also demonstrated in Li's work. A conductive ink made of silver nanoparticles was used to connect the current collectors of different printed supercapacitors, either in series or in parallel, in order to increase the output current. The array of supercapacitors was then used to light a series of LEDs, demonstrating the great potential held by DIW for integrated electronics.

Seol *et al.*[155] combined direct ink writing and fused deposition modelling to fabricate all the components of a solid-state interdigitated supercapacitor (Fig. 17g). Fused deposition modelling was used to print the device substrate, which consisted of ABS polymer with a layer of PVA on the top to reduce the surface roughness. A commercial Ag ink was printed onto the PVA layer *via* DIW to realize the current collector. Two different formulations were employed to print the electrodes: an activated carbon ink containing polymeric binders and conductive fillers was used to print electric-double-layer (EDL) supercapacitors, while a Mn_3O_4–graphene inks, containing carbon nanotubes as conductive filler and ethyl-cellulose as binder, was used to print pseudocapacitors. After printing, the structures were dried and a gel electrolyte ($LiClO_4$ and PVDF in propylene carbonate) was deposited on the top of the electrodes.[155] The EDL supercapacitors presented larger capacitance drop at high currents than non-printed devices, which was attributed to the larger amount of polymeric binder used to make the slurry printable. Accordingly, the printed pseudocapacitors presented better rate performance than the EDL supercapacitors, as a result of the smaller amount of binder used.[155]

Although the first printed device realized *via* DIW was a Li-ion battery,[53] the development of printed supercapacitors has rapidly surpassed batteries, providing numerous examples of all-printed systems. The reason for this probably lays in the inert environment required to test Li-based batteries rather than a direct technological advantage in printing supercapacitors. The use of different deposition techniques in the same manufacturing process has also been demonstrated,[155] representing a possible strategy to overcome the limits of an individual printing techniques in the fabrication of all-printed energy devices.

Conclusions and outlook

Originally developed for the additive manufacturing of ceramics, DIW is now gaining growing interest for energy applications, widening the spectrum of materials which can be printed. The formulation of printable inks from energy materials, which present the strict rheological requirements needed to build complex architectures and do not necessitate thermal post processing, represent the most pressing challenges for materials formulation. Additionally, technological advancement for the realization of multi-material printing at reduced production times is still necessary to make additive manufacturing competitive to serial production. In this review, the specific rheological prerequisites that inks should exhibit to print electrodes, electrolytes and separators as constituents of batteries, supercapacitors and electrocatalytic devices have been critically discussed. The strategies proposed in recent literature to meet the rheological requirements for printability and to attain 3D structures with high mechanical integrity have been discussed, highlighting the advantages and limitations of different approaches. Finally, the possibility to integrate different materials formulations to fabricate all-printed devices, reducing the cost and complexity of the manufacturing process, has been addressed. Ultimately, we have provided guidelines to improve the composition, printability, functionality and integration of inks for energy devices.

Although significant progress has been made in the development of new ink formulations and in the fabrication of all-printed devices, the potential of DIW for energy materials has yet to be fully explored. In particular, DIW offers the possibility to fabricate structures with arbitrary complexity, but only a limited number of geometries and device configurations has been investigated for energy applications thus far. Often, they are inspired by devices based on thin-films. Further research on the optimization of 3D

printed architectures to enhance the electrochemical performance, durability and mechanical strength of energy devices is needed. The printability of the inks and the electrochemical properties of the final device are both strongly influenced by the ink composition. Nonetheless, the assessment of the optimal ink formulation in terms of printability and electrochemical performance is often difficult, and quantitative models to evaluate the quality of inks treat the printability and electrical properties as unrelated quantities. A holistic description is needed to directly compare different compositions and promote the development of new ink formulations with predictable functional properties.

In addition to multi-material printing in a single processing step, DIW also offers the possibility to fabricate structures with gradient composition. A similar feature has not yet been exploited in printed energy devices and in the future, it could provide a further degree of freedom in the design of the electrodes. Higher amounts of active material could be deposited where the electrical current density is expected to be higher, such as at the edges of interdigitated structures, in order to increase the specific capacitance and cyclability.

In summary, the rheology and the functional composition of inks for DIW fabrication of energy materials is fast moving field which can unleash the full potential of this manufacturing technique. Detailed characterization of ink rheology, and sharing such information are necessary aspects to enable a rapid progression of the field. DIW deposition is only at the early stages of its use for energy applications at different length scales and it holds an enormous potential to revolutionize device architecture and performance to enable a wide-spread use of those in different technologies. Furthermore, multi-material printing in a single step and an increase in prototyping speed could lead to produce large batches of devices and thus making this technique suitable for large scale production on demand.

Conflicts of interest

There are no conflicts to declare.

Acknowledgements

C. M. would like to acknowledge the award of funding from the European Research Council (ERC) under the European Union' s Horizon 2020 research and innovation programme (Grant Agreement No. 819069) and the award of a Royal Society University Research Fellowship (UF160539) by the UK Royal Society.

References

1 M. R. Hartings and Z. Ahmed, *Nat. Rev. Chem.*, 2019, **3**, 305–314.
2 J. Kim, R. Kumar, A. J. Bandodkar and J. Wang, *Adv. Electron. Mater.*, 2017, **3**, 1–15.
3 M. Zeng and Y. Zhang, *J. Mater. Chem. A*, 2019, **7**(41), 23301–23336, DOI: 10.1039/C9TA07552F.
4 X. Tang, C. Zhu, D. Cheng, H. Zhou, X. Liu, P. Xie, Q. Zhao, D. Zhang and T. Fan, *Adv. Funct. Mater.*, 2018, **28**, 1–10.
5 T. Wang, X. Tian, L. Li, L. Lu, S. Hou, G. Cao and H. Jin, *J. Mater. Chem. A*, 2020, **8**(4), 1749–1756, DOI: 10.1039/C9TA11386J.
6 B. Yao, S. Chandrasekaran, H. Zhang, A. Ma, J. Kang, L. Zhang, X. Lu, F. Qian, C. Zhu, E. B. Duoss, C. M. Spadaccini, M. A. Worsley and Y. Li, *Adv. Mater.*, 2020, **32**, 1–10.
7 C.-Y. Lee, A. C. Taylor, A. Nattestad, S. Beirne and G. G. Wallace, *Joule*, 2019, **3**, 1835–1849.
8 C. Zhu, Z. Qi, V. A. Beck, M. Luneau, J. Lattimer, W. Chen, M. A. Worsley, J. Ye, E. B. Duoss, C. M. Spadaccini, C. M. Friend and J. Biener, *Sci. Adv.*, 2018, **4**(8), DOI: 10.1126/sciadv.aas9459.
9 M. Cheng, R. Deivanayagam and R. Shahbazian-Yassar, *Batteries Supercaps*, 2020, **3**, 130–146.
10 P. Chang, H. Mei, S. Zhou, K. G. Dassios and L. Cheng, *J. Mater. Chem. A*, 2019, **7**, 4230–4258.
11 M. Zhang, H. Mei, P. Chang and L. Cheng, *J. Mater. Chem. A*, 2020, **8**, 10670–10694.
12 Y. Zhang, G. Shi, J. Qin, S. E. Lowe, S. Zhang, H. Zhao and Y. L. Zhong, *ACS Appl. Electron. Mater.*, 2019, **1**, 1718–1734.
13 V. Egorov, U. Gulzar, Y. Zhang, S. Breen and C. O'Dwyer, *Adv. Mater.*, 2020, **2000556**, 1–27.
14 Y. Pang, Y. Cao, Y. Chu, M. Liu, K. Snyder, D. MacKenzie and C. Cao, *Adv. Funct. Mater.*, 2020, **30**, 1–22.
15 J. Sha, Y. Li, R. Villegas Salvatierra, T. Wang, P. Dong, Y. Ji, S.-K. Lee, C. Zhang, J. Zhang, R. H. Smith, P. M. Ajayan, J. Lou, N. Zhao and J. M. Tour, *ACS Nano*, 2017, **11**, 6860–6867.
16 D. R. Bourell, H. L. Marcus, J. W. Barlow and J. J. Beaman, *Int. J. Powder Metall.*, 1992, **28**(4), 369–383.
17 X. Zheng, H. Lee, T. H. Weisgraber, M. Shusteff, J. DeOtte, E. B. Duoss, J. D. Kuntz, M. M. Biener, Q. Ge, J. A. Jackson, S. O. Kucheyev, N. X. Fang and C. M. Spadaccini, *Science*, 2014, **344**, 1373–1377.
18 R. M. Hensleigh, H. Cui, J. S. Oakdale, J. C. Ye, P. G. Campbell, E. B. Duoss, C. M. Spadaccini, X. Zheng and M. A. Worsley, *Mater. Horiz.*, 2018, **5**, 1035–1041.
19 J. R. Tumbleston, D. Shirvanyants, N. Ermoshkin, R. Januszewicz, A. R. Johnson, D. Kelly, K. Chen, R. Pinschmidt, J. P. Rolland, A. Ermoshkin, E. T. Samulski and J. M. DeSimone, *Science*, 2015, **347**, 1349–1352, DOI: 10.1126/science.aaa2397.
20 L. Nayak, S. Mohanty, S. K. Nayak and A. Ramadoss, *J. Mater. Chem. C*, 2019, **7**, 8771–8795.
21 H. Minemawari, T. Yamada, H. Matsui, J. Tsutsumi, S. Haas, R. Chiba, R. Kumai and T. Hasegawa, *Nature*, 2011, **475**, 364–367.
22 J. Heinzl and C. H. Hertz, in *Ink-Jet Printing*, ed. P. W. Hawkes, 1985, pp. 91–171, https://doi.org/10.1016/S0065-2539(08)60877-X.
23 L. J. Deiner and T. L. Reitz, *Adv. Eng. Mater.*, 2017, **19**, 1600878.
24 C. (John) Zhang, L. McKeon, M. P. Kremer, S. H. Park, O. Ronan, A. Seral-Ascaso, S. Barwich, C. Coileáin, N. McEvoy, H. C. Nerl, B. Anasori, J. N. Coleman, Y. Gogotsi and V. Nicolosi, *Nat. Commun.*, 2019, **10**, 1–9.

25 D. Kong, L. T. Le, Y. Li, J. L. Zunino and W. Lee, *Langmuir*, 2012, **28**, 13467–13472.
26 F. Zhang, M. Wei, V. V. Viswanathan, B. Swart, Y. Shao, G. Wu and C. Zhou, *Nano Energy*, 2017, **40**, 418–431.
27 N. M. Farandos, L. Kleiminger, T. Li, A. Hankin and G. H. Kelsall, *Electrochim. Acta*, 2016, **213**, 324–331.
28 A. Zocca, P. Colombo, C. M. Gomes and J. Günster, *J. Am. Ceram. Soc.*, 2015, **98**, 1983–2001.
29 S. S. Crump, *ASME Annual Winter Conference*, PED, 1991, vol. 50, pp. 53–60.
30 X. Wei, D. Li, W. Jiang, Z. Gu, X. Wang, Z. Zhang and Z. Sun, *Sci. Rep.*, 2015, **5**, 11181.
31 G. I. J. Salentijn, P. E. Oomen, M. Grajewski and E. Verpoorte, *Anal. Chem.*, 2017, **89**, 7053–7061.
32 J. A. Lewis, *Adv. Funct. Mater.*, 2006, **16**, 2193–2204.
33 G. M. Gratson and J. A. Lewis, *Langmuir*, 2005, **21**, 457–464.
34 G. M. Gratson, M. Xu and J. A. Lewis, *Nature*, 2004, **428**, 386.
35 G. M. Gratson, F. García-Santamaría, V. Lousse, M. Xu, S. Fan, J. A. Lewis and P. V. Braun, *Adv. Mater.*, 2006, **18**, 461–465.
36 A. Corker, H. C. H. Ng, R. J. Poole and E. García-Tuñón, *Soft Matter*, 2019, **15**, 1444–1456.
37 M. Champeau, D. A. Heinze, T. N. Viana, E. R. de Souza, A. C. Chinellato and S. Titotto, *Adv. Funct. Mater.*, 2020, 1910606.
38 N. A. Kyerematen, T. Brousse and D. Pech, *Nat. Nanotechnol.*, 2017, **12**, 7–15.
39 H. Li and J. Liang, *Adv. Mater.*, 2019, **1805864**, 1805864.
40 S. Ferrari, M. Loveridge, S. D. Beattie, M. Jahn, R. J. Dashwood and R. Bhagat, *J. Power Sources*, 2015, **286**, 25–46.
41 S. Zheng, X. Shi, P. Das, Z. S. Wu and X. Bao, *Adv. Mater.*, 2019, **31**, 1–24.
42 J. T. Muth, P. G. Dixon, L. Woish, L. J. Gibson and J. A. Lewis, *Proc. Natl. Acad. Sci. U. S. A.*, 2017, **114**, 1832–1837.
43 E. Feilden, E. G. T. Blanca, F. Giuliani, E. Saiz and L. Vandeperre, *J. Eur. Ceram. Soc.*, 2016, **36**, 2525–2533.
44 S. S. Nadkarni and J. E. Smay, *J. Am. Ceram. Soc.*, 2006, **89**, 96–103.
45 C. Zhu, A. J. Pascall, N. Dudukovic, M. A. Worsley, J. D. Kuntz, E. B. Duoss and C. M. Spadaccini, *Annu. Rev. Chem. Biomol. Eng.*, 2019, **10**(1), 17–42, DOI: 10.1146/annurev-chembioeng-060718-030133.
46 C. Zhu and J. E. Smay, *J. Rheol.*, 2011, **55**, 655–672.
47 G. Pierin, C. Grotta, P. Colombo and C. Mattevi, *J. Eur. Ceram. Soc.*, 2016, **36**, 1589–1594.
48 Y. Eom, F. Kim, S. E. Yang, J. S. Son and H. G. Chae, *J. Rheol.*, 2019, **63**(2), 291–304, DOI: 10.1122/1.5058078.
49 H. A. Barnes, *J. Non-Newtonian Fluid Mech.*, 1997, **70**, 1–33.
50 H. Yuk and X. Zhao, *Adv. Mater.*, 2018, **30**, 1–8.
51 H. Zhou, P. He, P. Xie, Z. Cai, T. Fan, D. Cheng, X. Tang and D. Zhang, *ACS Nano*, 2018, **12**, 3502–3511.
52 Z. Qi, J. Ye, W. Chen, J. Biener, E. B. Duoss, C. M. Spadaccini, M. A. Worsley and C. Zhu, *Adv. Mater. Technol.*, 2018, **3**, 1–8.
53 K. Sun, T. S. Wei, B. Y. Ahn, J. Y. Seo, S. J. Dillon and J. A. Lewis, *Adv. Mater.*, 2013, **25**, 4539–4543.
54 L. Chen, X. Tang, P. Xie, J. Xu, Z. Chen, Z. Cai, P. He, H. Zhou, D. Zhang and T. Fan, *Chem. Mater.*, 2018, **30**, 799–806.
55 X. Tian, J. Jin, S. Yuan, C. K. Chua, S. B. Tor and K. Zhou, *Adv. Energy Mater.*, 2017, **7**, 1–17.
56 N. Liu and Y. Gao, *Small*, 2017, **13**, 1–10.
57 Y. Wang, C. Chen, H. Xie, T. Gao, Y. Yao, G. Pastel, X. Han, Y. Li, J. Zhao, K. (Kelvin) Fu and L. Hu, *Adv. Funct. Mater.*, 2017, **27**, 1703140.
58 H.-S. Min, B. Y. Park, L. Taherabadi, C. Wang, Y. Yeh, R. Zaouk, M. J. Madou and B. Dunn, *J. Power Sources*, 2008, **178**, 795–800.
59 K. Gerasopoulos, E. Pomerantseva, M. McCarthy, A. Brown, C. Wang, J. Culver and R. Ghodssi, *ACS Nano*, 2012, **6**, 6422–6432.
60 Z. Liang, Y. Pei, C. Chen, B. Jiang, Y. Yao, H. Xie, M. Jiao, G. Chen, T. Li, B. Yang and L. Hu, *ACS Nano*, 2019, **13**, 12653–12661.
61 T. Gao, Z. Zhou, J. Yu, J. Zhao, G. Wang, D. Cao, B. Ding and Y. Li, *Adv. Energy Mater.*, 2019, **9**, 1–10.
62 A. M'Barki, L. Bocquet and A. Stevenson, *Sci. Rep.*, 2017, **7**, 1–10.
63 J. E. Smay, J. Cesarano and J. A. Lewis, *Langmuir*, 2002, **18**, 5429–5437.
64 N. A. Dudukovic, L. L. Wong, D. T. Nguyen, J. F. Destino, T. D. Yee, F. J. Ryerson, T. Suratwala, E. B. Duoss and R. Dylla-Spears, *ACS Appl. Nano Mater.*, 2018, **1**, 4038–4044.
65 J. Orangi, F. Hamade, V. A. Davis and M. Beidaghi, *ACS Nano*, 2020, **14**, 640–650.
66 A. Z. Nelson and R. H. Ewoldt, *Soft Matter*, 2017, **13**, 7578–7594.
67 A. Z. Nelson, K. S. Schweizer, B. M. Rauzan, R. G. Nuzzo, J. Vermant and R. H. Ewoldt, *Curr. Opin. Solid State Mater. Sci.*, 2019, **23**, 100758.
68 P. Coussot, *J. Non-Newtonian Fluid Mech.*, 2014, **211**, 31–49.
69 A. T. Chan and J. A. Lewis, *Langmuir*, 2005, **21**, 8576–8579.
70 G. L. Hunter and E. R. Weeks, *Rep. Prog. Phys.*, 2012, **75**, 66501.
71 J. C. Conrad, S. R. Ferreira, J. Yoshikawa, R. F. Shepherd, B. Y. Ahn and J. A. Lewis, *Curr. Opin. Colloid Interface Sci.*, 2011, **16**, 71–79.
72 E. Zaccarelli, *J. Phys.: Condens. Matter*, 2007, **19**, 323101.
73 W. Yang, J. Yang, J. J. Byun, F. P. Moissinac, J. Xu, S. J. Haigh, M. Domingos, M. A. Bissett, R. A. W. Dryfe and S. Barg, *Adv. Mater.*, 2019, **31**, 1–8.
74 Y. Jiang, Z. Xu, T. Huang, Y. Liu, F. Guo, J. Xi, W. Gao and C. Gao, *Adv. Funct. Mater.*, 2018, **28**, 1–8.
75 V. G. Rocha, E. García-Tuñón, C. Botas, F. Markoulidis, E. Feilden, E. D'Elia, N. Ni, M. Shaffer and E. Saiz, *ACS Appl. Mater. Interfaces*, 2017, **9**, 37136–37145.
76 D. Cao, Y. Xing, K. Tantratian, X. Wang, Y. Ma, A. Mukhopadhyay, Z. Cheng, Q. Zhang, Y. Jiao, L. Chen and H. Zhu, *Adv. Mater.*, 2019, **31**, 1–10.
77 J. C. Conrad and J. A. Lewis, *Langmuir*, 2008, **24**, 7628–7634.
78 M. T. Roberts, A. Mohraz, K. T. Christensen and J. A. Lewis, *Langmuir*, 2007, **23**, 8726–8731.

79 C. Zhu and J. E. Smay, *J. Mater. Process. Technol.*, 2012, **212**, 727–733.
80 J. Mewis and N. J. Wagner, *Colloidal Suspension Rheology*, Cambridge University Press, 2011.
81 S. D. Lacey, D. J. Kirsch, Y. Li, J. T. Morgenstern, B. C. Zarket, Y. Yao, J. Dai, L. Q. Garcia, B. Liu, T. Gao, S. Xu, S. R. Raghavan, J. W. Connell, Y. Lin and L. Hu, *Adv. Mater.*, 2018, **30**, 1–9.
82 M. Dinkgreve, J. Paredes, M. M. Denn and D. Bonn, *J. Non-Newtonian Fluid Mech.*, 2016, **238**, 233–241.
83 B. Nan, F. J. Galindo-Rosales and J. M. F. Ferreira, *Mater. Today*, 2020, **xxx**, 1–9.
84 L. Martinie, H. Buggisch and N. Willenbacher, *J. Rheol.*, 2013, **57**, 627–646.
85 N. Louvet, D. Bonn and H. Kellay, *Phys. Rev. Lett.*, 2014, **113**, 218302.
86 K. Shen, H. Mei, B. Li, J. Ding and S. Yang, *Adv. Energy Mater.*, 2018, **8**, 1–6.
87 G. Hu, J. Kang, L. W. T. Ng, X. Zhu, R. C. T. Howe, C. G. Jones, M. C. Hersam and T. Hasan, *Chem. Soc. Rev.*, 2018, **47**, 3265–3300.
88 L. Wang, S. Chen, T. Shu and X. Hu, *ChemSusChem*, 2020, **13**, 1330–1353.
89 J. A. Lewis and G. M. Gratson, *Mater. Today*, 2004, **7**, 32–39.
90 D. W. McOwen, S. Xu, Y. Gong, Y. Wen, G. L. Godbey, J. E. Gritton, T. R. Hamann, J. Dai, G. T. Hitz, L. Hu and E. D. Wachsman, *Adv. Mater.*, 2018, **30**, 1–7.
91 C. Zhang, K. Shen, B. Li, S. Li and S. Yang, *J. Mater. Chem. A*, 2018, **6**, 19960–19966.
92 K. Fu, Y. Wang, C. Yan, Y. Yao, Y. Chen, J. Dai, S. Lacey, Y. Wang, J. Wan, T. Li, Z. Wang, Y. Xu and L. Hu, *Adv. Mater.*, 2016, **28**, 2587–2594.
93 L. Yu, L. Hu, B. Anasori, Y.-T. Liu, Q. Zhu, P. Zhang, Y. Gogotsi and B. Xu, *ACS Energy Lett.*, 2018, **3**, 1597–1603.
94 F. Kim, B. Kwon, Y. Eom, J. E. Lee, S. Park, S. Jo, S. H. Park, B.-S. Kim, H. J. Im, M. H. Lee, T. S. Min, K. T. Kim, H. G. Chae, W. P. King and J. S. Son, *Nat. Energy*, 2018, **3**, 301–309.
95 H. Zheng, R. Yang, G. Liu, X. Song and V. S. Battaglia, *J. Phys. Chem. C*, 2012, **116**, 4875–4882.
96 K. Tagawa and R. J. Brodd, in *Lithium-Ion Batteries: Science and Technologies*, ed. M. Yoshio, R. J. Brodd and A. Kozawa, Springer New York, New York, NY, 2009, pp. 181–194.
97 M. Cheng, Y. Jiang, W. Yao, Y. Yuan, R. Deivanayagam, T. Foroozan, Z. Huang, B. Song, R. Rojaee, T. Shokuhfar, Y. Pan, J. Lu and R. Shahbazian-Yassar, *Adv. Mater.*, 2018, **30**, 1–10.
98 R. R. Kohlmeyer, A. J. Blake, J. O. Hardin, E. A. Carmona, J. Carpena-Núñez, B. Maruyama, J. Daniel Berrigan, H. Huang and M. F. Durstock, *J. Mater. Chem. A*, 2016, **4**, 16856–16864.
99 Y. Liu, B. Zhang, Q. Xu, Y. Hou, S. Seyedin, S. Qin, G. G. Wallace, S. Beirne, J. M. Razal and J. Chen, *Adv. Funct. Mater.*, 2018, **28**, 1–12.
100 J. Kim, L. J. Cote, F. Kim, W. Yuan, K. R. Shull and J. Huang, *J. Am. Chem. Soc.*, 2010, **132**, 8180–8186.
101 A. Bagri, C. Mattevi, M. Acik, Y. J. Chabal, M. Chhowalla and V. B. Shenoy, *Nat. Chem.*, 2010, **2**, 581–587.
102 C. Mattevi, G. Eda, S. Agnoli, S. Miller, K. A. Mkhoyan, O. Celik, D. Mastrogiovanni, G. Granozzi, E. Garfunkel and M. Chhowalla, *Adv. Funct. Mater.*, 2009, **19**, 2577–2583.
103 G. Eda, J. Ball, C. Mattevi, M. Acik, L. Artiglia, G. Granozzi, Y. Chabal, T. D. Anthopoulos and M. Chhowalla, *J. Mater. Chem.*, 2011, **21**, 11217–11223.
104 S. Barg, F. M. Perez, N. Ni, P. do Vale Pereira, R. C. Maher, E. Garcia-Tuñon, S. Eslava, S. Agnoli, C. Mattevi and E. Saiz, *Nat. Commun.*, 2014, **5**, 4328.
105 S. Naficy, R. Jalili, S. H. Aboutalebi, R. A. Gorkin, K. Konstantinov, P. C. Innis, G. M. Spinks, P. Poulin and G. G. Wallace, *Mater. Horiz.*, 2014, **1**, 326–331.
106 E. García-Tuñón, E. Feilden, H. Zheng, E. D'Elia, A. Leong and E. Saiz, *ACS Appl. Mater. Interfaces*, 2017, 32977–32989.
107 M. Acik, C. Mattevi, C. Gong, G. Lee, K. Cho, M. Chhowalla and Y. J. Chabal, *ACS Nano*, 2010, **4**, 5861–5868.
108 A. Bagri, R. Grantab, N. V. Medhekar and V. B. Shenoy, *J. Phys. Chem. C*, 2010, **114**, 12053–12061.
109 W. Li, Y. Li, M. Su, B. An, J. Liu, D. Su, L. Li, F. Li and Y. Song, *J. Mater. Chem. A*, 2017, **5**, 16281–16288.
110 E. García-Tuñón, S. Barg, J. Franco, R. Bell, S. Eslava, E. D. Elia, R. C. Maher, F. Guitian and E. Saiz, *Adv. Mater.*, 2015, 1688–1693.
111 C. Gómez-Navarro, J. C. Meyer, R. S. Sundaram, A. Chuvilin, S. Kurasch, M. Burghard, K. Kern and U. Kaiser, *Nano Lett.*, 2010, **10**, 1144–1148.
112 P. C. Sherrell and C. Mattevi, *Mater. Today*, 2016, **19**, 428–436.
113 C. Zhu, T. Y. J. Han, E. B. Duoss, A. M. Golobic, J. D. Kuntz, C. M. Spadaccini and M. A. Worsley, *Nat. Commun.*, 2015, **6**, 1–8.
114 M. A. Worsley, S. Charnvanichborikarn, E. Montalvo, S. J. Shin, E. D. Tylski, J. P. Lewicki, A. J. Nelson, J. H. Satcher Jr., J. Biener, T. F. Baumann and S. O. Kucheyev, *Adv. Funct. Mater.*, 2014, **24**, 4259–4264.
115 C. Zhu, T. Liu, F. Qian, T. Y. J. Han, E. B. Duoss, J. D. Kuntz, C. M. Spadaccini, M. A. Worsley and Y. Li, *Nano Lett.*, 2016, **16**, 3448–3456.
116 L. Dong, J. Yang, M. Chhowalla and K. P. Loh, *Chem. Soc. Rev.*, 2017, **46**, 7306–7316.
117 J. Ma, P. Wang, L. Dong, Y. Ruan and H. Lu, *J. Colloid Interface Sci.*, 2019, **534**, 12–19.
118 L. Dong, Z. Chen, S. Lin, K. Wang, C. Ma and H. Lu, *Chem. Mater.*, 2017, **29**, 564–572.
119 Y. Z. Zhang, Y. Wang, Q. Jiang, J. K. El-Demellawi, H. Kim and H. N. Alshareef, *Adv. Mater.*, 2020, **32**, 1–26.
120 A. D. Dillon, M. J. Ghidiu, A. L. Krick, J. Griggs, S. J. May, Y. Gogotsi, M. W. Barsoum and A. T. Fafarman, *Adv. Funct. Mater.*, 2016, **26**, 4162–4168.
121 B. Akuzum, K. Maleski, B. Anasori, P. Lelyukh, N. J. Alvarez, E. C. Kumbur and Y. Gogotsi, *ACS Nano*, 2018, **12**, 2685–2694.
122 L. Yu, Z. Fan, Y. Shao, Z. Tian, J. Sun and Z. Liu, *Adv. Energy Mater.*, 2019, **9**, 1–8.
123 C. J. Zhang, S. Pinilla, N. McEvoy, C. P. Cullen, B. Anasori, E. Long, S.-H. Park, A. Seral-Ascaso, A. Shmeliov, D. Krishnan,

C. Morant, X. Liu, G. S. Duesberg, Y. Gogotsi and V. Nicolosi, *Chem. Mater.*, 2017, **29**, 4848–4856.
124 Y. Gogotsi and B. Anasori, *ACS Nano*, 2019, **13**, 8491–8494.
125 Z. Wang, Q. Zhang, S. Long, Y. Luo, P. Yu, Z. Tan, J. Bai, B. Qu, Y. Yang, J. Shi, H. Zhou, Z. Y. Xiao, W. Hong and H. Bai, *ACS Appl. Mater. Interfaces*, 2018, **10**, 10437–10444.
126 K. Shen, J. Ding and S. Yang, *Adv. Energy Mater.*, 2018, **8**(20), 1800408, DOI: 10.1002/aenm.201800408.
127 J. Zhao, Y. Zhang, X. Zhao, R. Wang, J. Xie, C. Yang, J. Wang, Q. Zhang, L. Li, C. Lu and Y. Yao, *Adv. Funct. Mater.*, 2019, **29**, 1900809.
128 Y. Qiao, Y. Liu, C. Chen, H. Xie, Y. Yao, S. He, W. Ping, B. Liu and L. Hu, *Adv. Funct. Mater.*, 2018, **28**, 1–7.
129 B. Yao, S. Chandrasekaran, J. Zhang, W. Xiao, F. Qian, C. Zhu, E. B. Duoss, C. M. Spadaccini, M. A. Worsley and Y. Li, *Joule*, 2019, **3**, 459–470.
130 Z. Wang, Y. Lee, S. Kim, J. Seo, S. Lee and L. Nyholm, *Adv. Mater.*, 2020, 2000892, DOI: 10.1002/adma.202000892.
131 L. Zhou, W. Ning, C. Wu, D. Zhang, W. Wei, J. Ma, C. Li and L. Chen, *Adv. Mater. Technol.*, 2019, **4**(2), 1800402, DOI: 10.1002/admt.201800402.
132 J. S. Park, T. Kim and W. S. Kim, *Sci. Rep.*, 2017, **7**, 1–10.
133 M. Drews, S. Tepner, P. Haberzettl, H. Gentischer, W. Beichel, M. Breitwieser, S. Vierrath and D. Biro, *RSC Adv.*, 2020, **10**, 22440–22448.
134 F. Hoeng, A. Denneulin and J. Bras, *Nanoscale*, 2016, **8**, 13131–13154.
135 S. R. Shin, R. Farzad, A. Tamayol, V. Manoharan, P. Mostafalu, Y. S. Zhang, M. Akbari, S. M. Jung, D. Kim, M. Comotto, N. Annabi, F. E. Al-Hazmi, M. R. Dokmeci and A. Khademhosseini, *Adv. Mater.*, 2016, **28**, 3280–3289.
136 C. Chaibundit, N. M. P. S. Ricardo, F. de, M. L. L. Costa, S. G. Yeates and C. Booth, *Langmuir*, 2007, **23**, 9229–9236.
137 Z. Lyu, G. J. H. Lim, R. Guo, Z. Kou, T. Wang, C. Guan, J. Ding, W. Chen and J. Wang, *Adv. Funct. Mater.*, 2019, **29**, 1–8.
138 H. Yuk, B. Lu, S. Lin, K. Qu, J. Xu, J. Luo and X. Zhao, *Nat. Commun.*, 2020, **11**, 4–11.
139 E. Koos and N. Willenbacher, *Science*, 2011, **331**, 897–900.
140 F. Bossler and E. Koos, *Langmuir*, 2016, **32**, 1489–1501.
141 C. Minas, D. Carnelli, E. Tervoort and A. R. Studart, *Adv. Mater.*, 2016, **28**, 9993–9999.
142 M. Schneider, E. Koos and N. Willenbacher, *Nat. Publ. Gr.*, 2016, 1–10.
143 H. Ding, S. Barg and B. Derby, *Nanoscale*, 2020, **12**, 11440–11447.
144 U. Daalkhaijav, O. D. Yirmibesoglu, S. Walker and Y. Mengüç, *Adv. Mater. Technol.*, 2018, **3**, 1700351.
145 S. B. Walker and J. A. Lewis, *J. Am. Chem. Soc.*, 2012, **134**, 1419–1421.
146 M. A. Skylar-Scott, J. Mueller, C. W. Visser and J. A. Lewis, *Nature*, 2019, **575**, 330–335.
147 J. O. Hardin, T. J. Ober, A. D. Valentine and J. A. Lewis, *Adv. Mater.*, 2015, **27**, 3279–3284.
148 E. Peng, D. Zhang and J. Ding, *Adv. Mater.*, 2018, **30**, 1–14.
149 G. J. H. Lim, Z. Lyu, X. Zhang, J. J. Koh, Y. Zhang, C. He, S. Adams, J. Wang and J. Ding, *J. Mater. Chem. A*, 2020, **8**, 9058–9067.
150 C. Chae, J. H. Han, S. S. Lee, Y. Choi, T. H. Kim and S. Jeong, *Adv. Funct. Mater.*, 2020, **2000715**, 1–10.
151 A. J. Blake, R. R. Kohlmeyer, J. O. Hardin, E. A. Carmona, B. Maruyama, J. D. Berrigan, H. Huang and M. F. Durstock, *Adv. Energy Mater.*, 2017, **7**, 1–10.
152 T. S. Wei, B. Y. Ahn, J. Grotto and J. A. Lewis, *Adv. Mater.*, 2018, **30**, 1–7.
153 K. Shen, J. Ding and S. Yang, *Adv. Energy Mater.*, 2018, **8**, 1800408.
154 G. Eda, G. Fanchini and M. Chhowalla, *Nat. Nanotechnol.*, 2008, **3**, 270–274.
155 M. L. Seol, I. Nam, E. L. Ribeiro, B. Segel, D. Lee, T. Palma, H. Wu, D. Mukherjee, B. Khomami, C. Hill, J. W. Han and M. Meyyappan, *ACS Appl. Energy Mater.*, 2020, **3**, 4965–4973.